CHEMISTRY OF MATERIALS

Article

pubs.acs.org/cm

Heteroleptic, Dinuclear Copper(I) Complexes for Application in Organic Light-Emitting Diodes

Daniel M. Zink,[†,‡] Daniel Volz,[†,‡] Thomas Baumann,*[,‡] Mathias Mydlak,[‡] Harald Flügge,[‡] Jana Friedrichs,[‡] Martin Nieger,[§] and Stefan Bräse*[,†,∥]

[†]Institute of Organic Chemistry, Karlsruhe Institute of Technology, KIT Campus South, Fritz-Haber-Weg 6, Karlsruhe D-76131, Germany

[‡]cynora GmbH, Hermann-von-Helmholtz-Platz 1, Eggenstein-Leopoldshafen D-76344, Germany

[§]Laboratory of Inorganic Chemistry, Department of Chemistry, University of Helsinki, P.O. Box 55 (A.I. Virtasen aukio 1), Helsinki FIN-00014, Finland

[∥]Institute of Toxicology and Genetics, Karlsruhe Institute of Technology (KIT), Hermann-von-Helmholtz-Platz 1, D-76344 Eggenstein-Leopoldshafen, Germany

S *Supporting Information*

ABSTRACT: A series of highly luminescent, heteroleptic copper(I) complexes has been synthesized using a modular approach based on easily accessible P^N ligands, triphenylphosphine, and copper(I) halides, allowing for an independent tuning of the emission wavelength with low synthetic efforts. The molecular structure has been investigated via X-ray analysis, confirming a dinuclear copper(I) complex consisting of a butterfly shaped metal-halide cluster and two different sets of ligands. The bidentate P^N ligand bridges the two metal centers and can be used to tune the energy of the frontier orbitals and therefore the photophysical characteristics, as confirmed by emission spectroscopy and theoretical investigations, whereas the two monodentate triphenylphosphine ligands on the periphery of the cluster core mainly influence the solubility of the complex. By using electron-rich or electron-poor heterocycles as part of the bridging ligand, emission colors can be adjusted, respectively, between yellow (581 nm) and deep blue (451 nm). These complexes have been further investigated in particular with regard to their photophysical properties in thin films and polymer matrix as well as in solution. Furthermore, the suitability of this class of materials for being applied in organic light-emitting diodes (OLEDs) has been demonstrated in a solution-processed device with a maximum current efficiency of 9 cd/A and a low turn-on voltage of 4.1 V using a representative complex as an emitting compound.

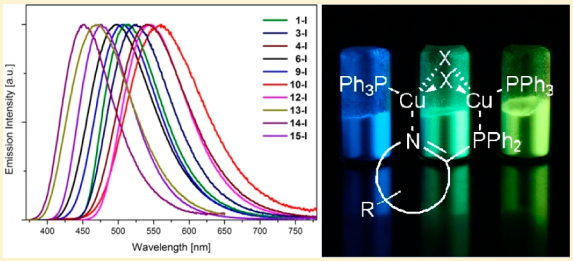

KEYWORDS: *copper, luminescence, cluster compounds, bridging ligands, P^N ligands, copper complexes, Cu(I) complexes, heteroleptic complexes, organic light-emitting diodes, dinuclear complexes*

1. INTRODUCTION

Organic light-emitting diodes (OLEDs) are highly attractive candidates for lighting and display applications because they offer numerous advantages such as enhanced efficiency and the possibility to be manufactured on thin and lightweight substrates.[1−6] Luminescent metal complexes containing Ir, Pt, or Os are widely used emitters for OLEDs not only because of their color tunability but also because of their high efficiencies.[7−26] However, these noble metals are rather scarce and expensive, which complicates their usage in high-volume productions. To enter mass market applications, luminescent complexes based on more abundant and cost-efficient metals with a d^{10} configuration, such as Cu(I), Ag(I), or Au(I), are currently in the focus of numerous research studies.[27−31] Among them, copper(I) complexes are favored not only because of their varied structural and photophysical properties but also because of the fact that they have already been successfully tested in OLEDs.[32−52]

After the pioneering work of McMillin and several other groups, mononuclear cationic copper(I) complexes have become well-known for their geometry change from a pseudotetrahedral coordination of the copper ion to a square planar coordination in the excited state. This flattening distortion is due to a formal oxidation from Cu(I) to Cu(II) upon excitation of these kinds of complexes.[37−51] This large structural rearrangement is regarded as the major quenching pathway of the emission and facilitates solvent coordination and exciplex formation, thus resulting in additional quenching pathways and leading to low quantum yields in solution.[53−56] By increasing the structural rigidity, these radiationless deactivation pathways can be reduced in mononuclear copper(I) complexes, leading to strongly enhanced quantum

Received: April 27, 2013
Revised: October 17, 2013

yields.[48,50,51] Rigid clusters containing more than one copper(I) ion are supposed to show a similar behavior.[46,57−59]

Recently a series of highly luminescent, homoleptic dinuclear copper(I) complexes was presented bearing three P^N ligands in the ligand sphere, which allows for a tuning of the emission color of the complexes by changing the electronic characteristics of the ligands.[32] These complexes feature high quantum yields[32] and are currently in the stage of device testing, resulting in high-performance OLEDs.[60]

After this analysis of the basic characteristics of these homoleptic complexes, two studies have been performed to investigate the influence of the single- and double-bound ligands. The first study aimed at minimizing the synthetic effort, by replacing the single-bound bidentate ligands on the periphery of the complex with commercially available phosphines, leading to new heteroleptic complexes that allow for an independent tuning of solubility and color. Various monodentate phosphines bearing solubility-enhancing groups were introduced, allowing for a fine-tuning of the solubility in different polar and apolar solvents, which is necessary for the production of solution-processed OLEDs. This study was recently published separately by Volz et al.[61]

In this consecutive study, the influence of the bidentate bridging ligand on the photophysical properties is investigated. A series of highly luminescent heteroleptic complexes is presented on the basis of a dinuclear copper(I) halide core, a bridging P^N ligand, and two triphenylphosphines as ancillary ligands. The structures of the complexes were revealed by X-ray structure analysis, confirming that the P^N ligand is bridging the two copper atoms, whereas the phosphines act as monodentate ligands. Density functional theory (DFT) calculations were performed showing that the highest occupied molecular orbital (HOMO) is mainly located on the copper(I) halide core, whereas the lowest unoccupied molecular orbital (LUMO) mainly resides on the bridging P^N ligand, thus allowing for an easy color tunability of the complexes. By changing the electronic characteristics of the bridging P^N ligand, the luminescence properties can be fine-tuned to cover almost the whole visible spectrum from deep blue (451 nm) to yellow (581 nm). In addition, the suitability of this modular emitter system for electronic applications has been demonstrated in a first solution-processed OLED device.

2. EXPERIMENTAL SECTION

2.1. General Procedures. Oven-dried glassware was used to perform all reactions under a nitrogen atmosphere. Solvents as well as chemicals employed were bought from commercial suppliers and applied without further purification. For thin-layer chromatography (TLC), silica gel plates (Silica gel 60, F254, Merck) were used with detection by UV. Preparative chromatography for purification was performed using normal-phase silica gel (Silica gel 60, 230−400 mesh, Merck).

2.2. Synthesis of P^N-Type Ligands. Ligands **1**−**5** were synthesized according to ref 32, and ligand **9** was synthesized according to ref 33. Precursors **28** and **29** were synthesized following the procedures reported by Kawano et al.[62] Spectroscopic data of ligands **1**,[63] **2**,[32] **3**,[32] **4**,[32] **9**,[64] and **10**[65] have already been published in the literature; for spectroscopic data of ligands **5**−**8** and **11**−**16**, see the Supporting Information.

*2.2.1. General Procedure for the Alkylation of 1,2,4-Triazoles, Yielding Compounds **19**−**21**.*[66] To a stirred solution of 1*H*-1,2,4-triazole (**18**) (29.0 mmol, 1.00 equiv) and the appropriate alkyl halide (30.4 mmol, 1.05 equiv) in tetrahydrofuran (25 mL) was added 1,8-diazabicyclo[5.4.0]undec-7-ene (34.8 mmol, 1.20 equiv) dissolved in tetrahydrofuran (5 mL) dropwise via cannula under a nitrogen atmosphere at room temperature. After stirring for 24 h at room temperature, the reaction mixture was quenched with water (100 mL) and extracted with dichloromethane (3 × 80 mL). The organic layers were combined, washed with brine (80 mL), and dried over $MgSO_4 \times H_2O$, and the solvent was removed under vacuum. The crude products were used without further purification.

*2.2.2. General Procedure for the Phosphorylation of Alkylated Compounds **19**−**21**, Yielding Compounds **6**−**8**.* A solution of the alkylated triazole precursor (8.67 mmol, 1.00 equiv) in dry tetrahydrofuran (20 mL) under a nitrogen atmosphere was cooled to −80 °C. To this solution, lithium diisopropylamine (1.8 M in tetrahydrofuran, 9.54 mmol, 1.10 equiv) was added dropwise via cannula. Afterward, the reaction was allowed to warm to 0 °C slowly. Subsequently, the reaction mixture was cooled to −80 °C again, and chlorodiphenylphosphane (9.54 mmol, 1.10 equiv) dissolved in tetrahydrofuran (10 mL) was added dropwise via cannula. The reaction mixture was allowed to warm to room temperature overnight, quenched with water (2 mL), and filtered through a plug of silica gel. Purification via flash column chromatography yielded the product.

*2.2.3. General Procedure for the Introduction of Alkyl (a) or Aryl[67] (b) Substituents at Imidazoles or Benzoimidazoles, Yielding Compounds **22**−**25**.* (a) To a solution of the appropriate benzoimidazole or imidazole (50.0 mmol, 1.00 equiv) and sodium hydroxide (55.0 mmol, 1.10 equiv) in dimethyl sulfoxide (100 mL) was added the alkyl halide (50.0 mmol, 1.00 equiv), and the reaction mixture was stirred at 40 °C overnight. Afterward, the reaction was quenched with water (200 mL). The aqueous layer was extracted with ethyl acetate (3 × 100 mL), and the combined organic layers were washed with water (3 × 100 mL) and dried over $MgSO_4 \times H_2O$. Removing of the solvent under reduced pressure yielded the crude product, which was used without further purification. (b) Benzoimidazole or imidazole (20.0 mmol, 1.00 equiv), 1,10-phenanthroline (4.00 mmol, 20 mol %), copper(I) iodide (2.00 mmol, 10 mol %), cesium carbonate (30.0 mmol, 1.50 equiv), and the corresponding aryl iodide or bromide (20.0 mmol, 1.00 equiv) were dissolved under a nitrogen atmosphere in dimethylformamide (35 mL) and stirred at 110 °C for 3 h. The reaction mixture was filtered through a plug of silica gel, and the crude product was further purified by flash column chromatography.

*2.2.4. General Procedure for the Phosphorylation of Compounds **22**−**25**, Yielding Compounds **12**−**16**.*[68] The appropriate alkylated or arylated benzimidazole or imidazole (15.2 mmol, 1.00 equiv) was dissolved in tetrahydrofuran (50 mL) under a nitrogen atmosphere and cooled to −78 °C, and *n*-butyllithium (2.5 min *n*-hexane, 16.7 mmol, 1.10 equiv) was added dropwise via cannula. The reaction mixture was stirred at −78 °C for 30 min followed by stirring at room temperature for 1 h. Afterward, the reaction mixture was cooled to −78 °C again, chlorodiphenylphosphane (16.0 mmol, 1.05 equiv) dissolved in tetrahydrofuran (10 mL) was added dropwise via cannula, and the reaction mixture was allowed to warm to room temperature overnight. After quenching with water (3 mL), the mixture was filtered through a plug of silica gel. Purification via flash column chromatography yielded the product.

*2.2.5. General Procedure for the Synthesis of Compounds **10** and **11**.* To a solution of oxadiazole (**28** or **29**) (3.61 mmol, 1.00 equiv) and triethylamine (14.4 mmol, 4.00 equiv) in pyridine (6 mL) chlorodiphenylphosphane (4.00 mmol, 1.10 equiv) was added dropwise via cannula under a nitrogen atmosphere, and the reaction mixture was stirred at room temperature for 24 h. After quenching with hydrochloric acid (1 M, 50 mL), the aqueous layer was extracted with dichloromethane (3 × 40 mL). The combined organic layers were dried over $MgSO_4 \times H_2O$, and the solvent was removed under reduced pressure. Purification via flash column chromatography yielded the product.

*2.2.6. General Procedure for the Synthesis of Complexes **1-I**−**15-I**, **1-Br**, and **1-Cl**.* The copper(I) halide salt (1.00 mmol, 2.00 equiv), the P^N ligand (0.50 mmol, 1.00 equiv), and the phosphine (1.00 mmol, 2.00 equiv) were suspended in dry dichloromethane (10 mL) under nitrogen. The reaction mixture was stirred for 12 h at room temperature, and the appropriate complex was purified afterward

dx.doi.org/10.1021/cm4018375 | *Chem. Mater.* XXXX, XXX, XXX−XXX

through precipitation with diethyl ether, pentane, or cyclohexane (100 mL). The precipitated solid was filtered off, further purified by washing with the appropriate solvent, and dried under vacuum.

*[(2-(Diphenylphosphino)pyridine)(PPh$_3$)$_2$Cu$_2$I$_2$] (**1-I**).* Yield: 969 mg, 0.83 mmol, 87%; yellow powder. IR (ATR) $\tilde{\nu}_{max}$: 3044 (vw), 1478 (w), 1433 (w), 1091 (w), 996 (w), 740 (m), 691 (m), 489 (m), 435 (w), 418 (w) cm^{-1}. MS (FAB): because of the insolubility of the compound, no mass spectra could be measured. Anal. Calcd for $C_{53}H_{44}Cu_2I_2NP_3$ (1166.9): C, 54.47; H, 3.79; N, 1.20. Found: C, 54.39; H, 3.79; N, 0.93.

*[(2-(Diphenylphosphino)pyridine)(PPh$_3$)$_2$Cu$_2$Br$_2$] (**1-Br**).* Yield: 977 mg, 0.91 mmol, 80%; yellow powder. IR (ATR) $\tilde{\nu}_{max}$: 1479 (w), 1451 (w), 1434 (w), 1092 (w), 1027 (w), 997 (w), 741 (m), 692 (m), 512 (m), 499 (m), 489 (m), 435 (w), 417 (w) cm^{-1}. MS (FAB): because of the insolubility of the compound, no mass spectra could be measured. Anal. Calcd for $C_{53}H_{44}Cu_2Br_2NP_3$ (1071.0): C, 59.23; H, 4.13; N, 1.30. Found: C, 58.91; H, 4.28; N, 1.03.

*[(2-(Diphenylphosphino)pyridine)(PPh$_3$)$_2$Cu$_2$Cl$_2$] (**1-Cl**).* Yield: 842 mg, 0.85 mmol, 75%; yellow powder. IR (ATR) $\tilde{\nu}_{max}$: 3045 (vw), 1479 (w), 1434 (w), 1094 (w), 742 (m), 692 (s), 513 (m), 500 (m), 435 (w), 419 (w) cm^{-1}. MS (FAB) *m*/*z* (%): 950 (1), 785 (2), 687 (17), 587 (45), 424 (12), 327 (8), 325 (30), 262 (35). Anal. Calcd for $C_{53}H_{44}Cl_2Cu_2NP_3$ (983.1): C, 64.57; H, 4.50; N, 1.42. Found: C, 64.22; H, 4.51, N, 1.16.

*[(2-(Diphenylphosphino)-4-methylpyridine)(PPh$_3$)$_2$Cu$_2$I$_2$] (**2-I**).* Yield: 555 mg, 0.87 mmol, 75%; yellow powder. IR (ATR) $\tilde{\nu}_{max}$: 3047 (vw), 1479 (w), 1433 (w), 1090 (w), 1026 (w), 997 (w), 827 (w), 740 (m), 692 (m), 512 (m), 490 (m), 462 (w) cm^{-1}. MS (FAB): because of the insolubility of the compound, no mass spectra could be measured. Anal. Calcd for $C_{54}H_{46}Cu_2I_2NP_3$ (1181.0): C, 54.84; H, 3.92; N, 0.83. Found: C, 54.45; H, 4.04; N, 0.79.

*[(2-(Diphenylphosphino)-4-propylpyridine)(PPh$_3$)$_2$Cu$_2$I$_2$] (**3-I**).* Yield: 912 mg, 0.75 mmol, 76%; yellow powder. IR (ATR) $\tilde{\nu}_{max}$: 3049 (vw), 2959 (vw), 1478 (w), 1458 (w), 1433 (w), 1390 (w), 1090 (w), 1027 (w), 997 (w), 742 (m), 692 (m), 508 (m), 486 (m) cm^{-1}. MS (FAB) *m*/*z* (%): 1055 (4), 863 (2), 750 (3), 630 (4), 560 (6), 368 (11). Anal. Calcd for $C_{56}H_{50}Cu_2I_2NP_3$ (1209.0): C, 55.55; H, 4.16; N, 1.16. Found: C, 55.53; H, 4.18; N, 0.83.

*[(2-(Diphenylphosphino)-4-isobutylpyridine)(PPh$_3$)$_2$Cu$_2$I$_2$] (**4-I**).* Yield: 1.85 g, 1.51 mmol, 96%; yellow powder. IR (ATR) $\tilde{\nu}_{max}$: 3050 (vw), 2954 (vw), 1597 (vw), 1479 (w), 1434 (w), 1385 (vw), 1363 (vw), 1094 (w), 1074 (w), 742 (w), 692 (m), 515 (m), 476 (w) cm^{-1}. MS (FAB) *m*/*z* (%): 1274 (11), 1083 (36), 893 (10), 836 (21), 763 (38), 644 (58), 572 (83), 515 (9), 382 (100), 324 (22). Anal. Calcd for $C_{57}H_{52}Cu_2I_2NP_3$ (1223.0): C, 55.89; H, 4.28; N, 1.14. Found: C, 55.53; H, 4.22; N, 0.82.

*[(2-(Diphenylphosphino)-4-(3-(2-methoxyethoxy)propyl)-pyridine)(PPh$_3$)$_2$Cu$_2$I$_2$] (**5-I**).* Yield: 880 mg, 0.68 mmol, 65%; yellow powder. IR (ATR) $\tilde{\nu}_{max}$: 3048 (vw), 2867 (vw), 1479 (w), 1433 (m), 1093 (m), 1027 (w), 998 (w), 741 (m), 692 (m), 516 (m), 430 (w) cm^{-1}. MS (FAB) *m*/*z* (%): 1202 (7), 894 (7), 824 (2), 704 (5), 632 (10), 587 (18), 442 (10), 380 (2), 325 (8). Anal. Calcd for $C_{59}H_{56}Cu_2I_2NO_2P_3$ (1283.0): C, 55.15; H, 4.39; N, 1.09. Found C, 54,75; H, 4.34; N, 0.74.

*[(5-(Diphenylphosphino)-1-propyl-1H-1,2,4-triazole)(PPh$_3$)$_2$Cu$_2$I$_2$] (**6-I**).* Yield: 1.11 g, 0.93 mmol, 91%; white powder. IR (ATR) $\tilde{\nu}_{max}$: 3049 (w), 1480 (w), 1432 (w), 1094 (w), 1028 (w), 744 (m), 693 (s), 670 (w), 519 (m), 506 (s), 493 (m), 452 (w) cm^{-1}. MS (FAB): because of the insolubility of the compound, no mass spectra could be measured. Anal. Calcd for $C_{53}H_{48}Cu_2I_2N_3P_3$ (1199.0): C, 53.01; H, 4.03; N, 3.50. Found: C, 52.77; H, 4.05; N, 3.11.

*[(5-(Diphenylphosphino)-1-pentyl-1H-1,2,4-triazole)(PPh$_3$)$_2$Cu$_2$I$_2$] (**7-I**).* Yield: 879 mg, 0.72 mmol, 77%; white powder. IR (ATR) $\tilde{\nu}_{max}$: 3049 (vw), 2927 (vw), 1479 (vw), 1431 (m), 1093 (w), 1027 (w), 997 (w), 741 (m), 691 (m), 520 (m), 504 (m), 490 (m), 461 (w), 422 (w) cm^{-1}. MS (FAB) *m*/*z* (%): 1414 (8), 1091 (30), 901 (25), 766 (41), 648 (33), 578 (95), 386 (100), 324 (83). Anal. Calcd for $C_{55}H_{52}Cu_2I_2N_3P_3$ (1227.0): C, 53.76; H, 4.27; N, 3.42. Found: C, 53.52; H, 4.34; N, 3.51.

*[(1-Benzyl-5-(diphenylphosphino)-1H-1,2,4-triazole)(PPh$_3$)$_2$Cu$_2$I$_2$] (**8-I**).* Yield: 854 mg, 0.68 mmol, 78%; white powder. IR (ATR) $\tilde{\nu}_{max}$: 3050 (vw), 1479 (w), 1433 (m), 1093 (w), 740 (m), 721 (w), 691 (m), 516 (m), 504 (m) cm^{-1}. MS (FAB) *m*/*z* (%): 325 (44), 406 (100), 587 (70), 668 (80), 777 (28), 860 (27), 1120 (5). Anal. Calcd for $C_{57}H_{48}Cu_2I_2N_3P_3$ (1247.0): C, 54.82; H, 3.87; N, 3.36. Found: C, 54.67; H, 3.78; N, 3.28.

*[(4-(Diphenylphosphino)-1,5-diphenyl-1H-1,2,3-triazole)-(PPh$_3$)$_2$Cu$_2$I$_2$] (**9-I**).* Yield: 329 mg, 0.25 mmol, 81%; white powder. IR (ATR) $\tilde{\nu}_{max}$: 3044 (vw), 1480 (w), 1433 (m), 1156 (w), 1094 (m), 1028 (w), 998 (w), 773 (w), 740 (m), 690 (s), 608 (w), 520 (m), 502 (s), 486 (m), 438 (w) cm^{-1}. MS (FAB) *m*/*z* (%): 1255 (12), 1065 (1), 920 (5), 850 (11), 730 (5), 658 (12), 587 (10). Anal. Calcd for $C_{62}H_{50}Cu_2I_2N_3P_3$ (1309.0): C, 56.81; H, 3.84; N, 3.21. Found: C, 56.88; H, 3.85; N, 3.09.

*[(2-(Diphenylphosphino)-5-phenyl-1,3,4-oxadiazole)(PPh$_3$)$_2$Cu$_2$I$_2$] (**10-I**).* Yield: 844 mg, 0.68 mmol, 90%; yellow powder. IR (ATR) $\tilde{\nu}_{max}$: 3051 (vw), 1552 (w), 1480 (w), 1433 (w), 1342 (vw), 1094 (w), 1027 (w), 994 (w), 742 (m), 692 (s), 541 (m), 519 (m), 507 (m), 488 (m), 427 (w) cm^{-1}. MS (FAB): because of the insolubility of the compound, no mass spectra could be measured. Anal. Calcd for $C_{56}H_{45}Cu_2I_2N_2OP_3$ (1233.9): C, 54.43; H, 3.67; N, 2.27. Found: C, 54.45; H, 4.07; N, 1.97.

*[(2-(Diphenylphosphino)-5-p-tolyl-1,3,4-oxadiazole)(PPh$_3$)$_2$Cu$_2$I$_2$] (**11-I**).* Yield: 986 mg, 0.79 mmol, 91%; yellow powder. IR (ATR) $\tilde{\nu}_{max}$: 2969 (vw), 1497 (w), 1480 (w), 1434 (w), 1094 (w), 1078 (w), 741 (w), 692 (m), 625 (vw), 520 (w), 507 (m), 487 (w) cm^{-1}. MS (FAB) *m*/*z* (%): 1121 (<1), 943 (1), 861 (2), 777 (2), 669 (8), 597 (10). Anal. Calcd for $C_{57}H_{47}Cu_2I_2N_2OP_3 \cdot 1.5\ CH_2Cl_2$: C, 51.02; H, 3.66; N, 2.03. Found: C, 51.31; H, 3.71; N, 2.00.

*[(2-(Diphenylphosphino)-4,5-dimethylthiazole)(PPh$_3$)$_2$Cu$_2$I$_2$] (**12-I**).* Yield: 1.12 g, 0.93 mmol, 92%; yellow powder. IR (ATR) $\tilde{\nu}_{max}$: 3048 (vw), 1478 (w), 1432 (w), 1360 (vw), 1092 (w), 1027 (vw), 998 (vw), 849 (vw), 742 (w), 692 (m), 518 (w), 506 (w), 492 (m), 447 (w), 419 (w) cm^{-1}. MS (FAB): because of the insolubility of the compound, no mass spectra could be measured. Anal. Calcd for $C_{52}H_{46}Cu_2I_2NP_3S \cdot CH_2Cl_2$: C, 50.36; H, 3.76; N, 1.09; S, 2.49. Found: C, 50.31; H, 3.96; N, 0.86; S, 2.33.

*[(2-(Diphenylphosphino)-1-p-tolyl-1H-imidazole)(PPh$_3$)$_2$Cu$_2$I$_2$] (**13-I**).* Yield: 1.31 g, 1.05 mmol, 90%; white powder. IR (ATR) $\tilde{\nu}_{max}$: 3048 (vw), 1505 (w), 1479 (w), 1432 (m), 1305 (w), 1127 (w), 1092 (w), 1027 (w), 998 (w), 823 (w), 739 (m), 691 (s), 617 (w), 566 (w), 519 (m), 504 (s), 472 (m) cm^{-1}. MS (FAB) *m*/*z* (%): 1130 (5), 860 (<1), 787 (5), 595 (5), 405 (16). The crystal structure analysis showed the presence of one molecule of dichloromethane in the crystal. Therefore, the complex was precipitated and recrystallized again leading to a reduction of the incorporated dichloromethane. However, an elemental analysis without cocrystallized dichloromethane could not be achieved. Anal. Calcd for $C_{58}H_{49}Cu_2I_2N_2P_3 \cdot 0.25CH_2Cl_2$ (1246.0): C, 55.13; H, 3.93; N, 2.21. Found: C, 55.26; H, 4.02; N, 1.88.

*[(2-(Diphenylphosphino)-4-methyl-1-p-tolyl-1H-imidazole)-(PPh$_3$)$_2$Cu$_2$I$_2$] (**14-I**).* Yield: 590 mg, 0.47 mmol, 83%; white powder. IR (ATR) $\tilde{\nu}_{max}$: 3047 (vw), 1508 (w), 1478 (w), 1433 (m), 1398 (w), 1179 (vw), 1150 (vw), 1092 (w), 1028 (w), 997 (w), 821 (w), 742 (m), 693 (m), 503 (m), 490 (m), 424 (w) cm^{-1}. MS (FAB) *m*/*z* (%): 1156 (2), 965 (<1), 800 (<1), 419 (4). Anal. Calcd for $C_{59}H_{51}Cu_2I_2N_2P_3$: C, 56.16; H, 4.07; N, 2.22. Found: C, 55.78; H, 4.08; N, 2.05.

*[(2-(Diphenylphosphino)-5,6-dimethyl-1-octyl-1H-benzo[d]-imidazole)(PPh$_3$)$_2$Cu$_2$I$_2$] (**15-I**).* Yield: 542 mg, 0.34 mmol, 74%; white powder. IR (ATR) $\tilde{\nu}_{max}$: 3053 (vw), 2927 (vw), 1480 (w), 1434 (w), 1094 (w), 1028 (vw), 998 (vw), 872 (vw), 836 (vw), 742 (w), 693 (m), 519 (m), 490 (w), 463 (w), 433 (w) cm^{-1}. MS (FAB) *m*/*z* (%): 1329 (5), 948 (3), 768 (9), 695 (12), 587 (2), 506 (19), 443 (15). Anal. Calcd for $C_{65}H_{65}Cu_2I_2N_2P_3$ (1346.1): C, 57.91; H, 4.86; N, 2.08. Found: C, 57.60; H, 4.79; N, 1.93.

*[(2-(Diphenylphosphino)-5,6-dimethyl-1-p-tolyl-1H-benzo[d]-imidazole)(PPh$_3$)$_2$Cu$_2$I$_2$] (**16-I**).* Yield: 1.06 g, 0.80 mmol, 84%; white powder. IR (ATR) $\tilde{\nu}_{max}$: 3047 (vw), 1513 (w), 1479 (w), 1433 (m), 1400 (w), 1158 (w), 1093 (w), 1027 (w), 995 (w), 887 (w), 850 (w),

dx.doi.org/10.1021/cm4018375 | *Chem. Mater.* XXXX, XXX, XXX−XXX

811 (w), 740 (w), 690 (s), 520 (m), 506 (s), 488 (m) cm^{-1}. MS (FAB) m/z (%): 903 (10), 864 (15), 745 (18), 675 (54), 587 (15) 482 (100). Anal. Calcd for $C_{64}H_{55}Cu_2I_2N_2P_3$ (1324.0): C, 57.97; H, 4.18; N, 2.11. Found: C, 57.96; H, 4.32; N, 1.80.

2.3. X-ray Crystallography. The crystal structure determinations of **2-I**, **11-I**, **12-I**, **13-I**, **14-I**, and **16-I** were performed on a Bruker-Nonius Kappa CCD diffractometer at 123(2) K, a Bruker SMART APEXII diffractometer at 120(2) K (**16-I**), and a Bruker Apex Duo diffractometer at 120(K) (**13-I**) using Mo Kα radiation (λ = 0.71073 Å). Crystal data, data collection parameters, and results of the analyses are listed in Table S1 in the Supporting Information. Direct methods were used for structure solution (SHELXS-97),[69] and refinement was carried out using SHELXL-97 (full-matrix least-squares on F^2).[69] Hydrogen atoms were refined using a riding model. A semiempirical absorption correction using equivalent reflections was applied.

In **2-I**, the Cu(2) atom is disordered (s.o.f. = 0.94). In **11-I**, there are four voids around the center of symmetry with 1.5 disordered molecules CH_2Cl_2 in each void. The disorder could not be solved, and the diffuse electron density was treated using SQUEEZE (module in PLATON).[70]

2.4. Photophysical Measurements. A Horiba Scientific FluoroMax-4 spectrofluorometer equipped with a 150 W xenon-arc lamp, excitation and emission monochromators (1200 grooves/nm blazed at 330 nm (excitation) and 500 nm (emission)), a Hamamatsu R928 photomultiplier tube, and a TCSPC-option was used to measure steady-state as well as time-resolved emission spectra. Standard correction curves were employed to correct the emission and excitation spectra for source intensity (lamp and grating). Using the FM-2013 accessory and a Horiba Yvon Jobin TCSPC hub, decay-time measurements were recorded and detected on the same system. A NanoLED 370 (λ = 371 nm, 1.5 ns pulse) was used as the excitation source. The quality of the fit was warranted by minimizing the χ^2 function and by visual inspection of the weighted residuals. A Hamamatsu Photonics absolute PL quantum yield measurement system (C9920-02G) equipped with a L9799-01 CW Xenon light source (150 W), monochromator, C7473 photonic multichannel analyzer, and integrating sphere and employing U6039-05 PLQY measurement software (Hamamatsu Photonics, Ltd., Shizuoka, Japan) was employed to measure the photoluminescence quantum yields. A Thermo Scientific Evolution 201 UV−vis spectrophotometer was used for measuring UV−vis absorption spectra. All solvents used were of spectrometric grade. Degassed samples were prepared by purging with argon for 30 min.

2.5. Computational Methods. Complexes **2-I**, **12-I**, **13-I**, **14-I**, and **16-I** were studied using density functional theory (DFT). Initial geometries were obtained from single-crystal X-ray diffraction data (see above) and were optimized in the ground state and in the lowest triplet state using the BP86[71,72] functional with the resolution-of-identity (RI)[73−75] approximation. Analytical harmonic vibrational frequency calculations were performed to verify that the optimized structures are minima on the potential energy surface. Energies and frontier orbitals were also computed using the B3LYP[76,77] functional. Phosphorescence energies were calculated using the following approaches: (1) time-dependent DFT (TDDFT) with the B3LYP functional, (2) energy difference between the closed-shell singlet ground state and the lowest (unrestricted) triplet state (ΔSCF), and (3) using the spin-flip Tamm−Dancoff[78] approximation (SF-TDA). Ground-state geometries of ligands **1**−**16** were optimized using the B3LYP functional. In all calculations, the def2-SV(P) basis set[79,80] and the m4 grid for numerical integration were employed. All calculations were performed with the Turbomole program package, version 6.4.[81]

2.6. Electrochemistry. The measurements were performed on a model 600D series electrochemical analyzer with workstation, CH Instruments. At room temperature and under an argon atmosphere, experiments were carried out in a three-electrode cell, with a Pt-wire as counter electrode and Pt-disk electrodes as reference as well as working electrodes. As electrolyte, NBu_4PF_6 was used at a concentration of 10^{-1} M in dichloromethane. The concentration of the complex was 10^{-3} M. The potential of the quasi-reference electrode (Pt disk) was corrected to the Ag/AgCl reference by measuring the ferrocene/ferrocenium redox couple. Andersson's method was used to obtain values for the absolute HOMO energy out of the first oxidation process.[82] According to the method of Tauc, values for the LUMO energy can be approximated by adding the values for the HOMO and the optical band gaps.[83]

2.7. Device Fabrication and Characterization. OLED devices have been prepared starting from indium−tin-oxide (ITO)-covered glass substrates with a sheet resistance of 16 Ω/m^2. The substrates were cleaned in a 2% aqueous solution of Helmanex, washed with deionized water, and treated with ozone for 10 min prior to spin-coating with PEDOT:PSS (Heraeus AL4083) filtered through a 0.45 μm syringe filter. This layer was dried at 120 °C for 1 h in air. The following organic layers were deposited under an inert atmosphere from solutions passed through 0.45 μm syringe filters. A 17 nm poly-TPD film (Lumtec, Taiwan) was spin-coated from a chlorobenzene solution and annealed at 110 °C for 60 min. Subsequently, the emitting layer was deposited, consisting of compound **4-I**:TPBi:PVK (45:45:10), from a toluene solution, resulting in a 30 nm thick layer. After annealing at 80 °C for 10 min, the following layers were deposited by evaporation under vacuum: TPBi (30 nm), Ca (8 nm), and Ag (100 nm). The active area of the resulting device was 24 mm^2. Finally, the device was encapsulated using 3 M barrier foil. Current (J), voltage (V), and luminance (L) characteristics were measured with a BoTest System.

3. RESULTS AND DISCUSSION

3.1. Synthesis. Copper(I) complexes with either phosphane, pyridine, or bridging P^N ligands are well-known for their rich coordination chemistry including mono-, di-, tri-, tetra-, or polynuclear complexes.[46,84−91] These complexes can be prepared systematically by controlling the reaction stoichiometry.[46,92] On the basis of our experiences with dinuclear complexes containing three identical P^N ligands with one of them acting as a bridging ligand and the other as ancillary ligands, coordinated solely via their phosphorus atom, our approach was to substitute these two monodentate ligands with two commercially available triphenylphosphine ligands. This approach not only simplifies the synthetic effort dramatically but also is also very modular because the emission and the solubility can be tuned independently via the bridging ligand and the ancillary ligands, respectively. Herein, we report on the effects of the bridging ligand regarding the luminescence properties of the resulting complexes, and a detailed investigation of a variety of different ancillary ligands and their effects on the solubility and processability has been published separately.[61]

The P^N ligands studied in this work can be divided into diphenylphosphines with five- and six-member heterocycles, as shown in Chart 1. These ligands were chosen not only because of their different electronic characteristics arising from different heterocycles but also because of the possible facile introduction of substituents on the heterocycles to fine-tune either the solubility or the photophysical properties. Substituents with alkyl chains of different lengths and branching can be used to fine-tune solubility in nonpolar organic solvents such as chlorobenzene, toluene, xylene, or tetrahydrofuran, which are potential solvents for device mass-production because of their relatively high boiling points. The investigated complexes bear different heterocycles as part of the bridging ligand, namely, pyridine (**1**−**5**), 1,2,4-triazole (**6**−**8**), 1,2,3-triazole (**9**), oxadiazole (**10** and **11**), thiazole (**12**), imidazole (**13** and **14**), and benzimidazole (**15** and **16**) along with two triphenylphosphines as ancillary ligands (Chart 1). In addition, the introduction of alkyl and phenyl substituents on the heterocycles has been analyzed for the majority of the groups.

dx.doi.org/10.1021/cm4018375 | Chem. Mater. XXXX, XXX, XXX−XXX

Chart 1. Synthesized P^N Ligands Bearing Different Heterocycles to Tune the Emission Spectra of the Corresponding Complexes through Different Electronic Characteristics[a]

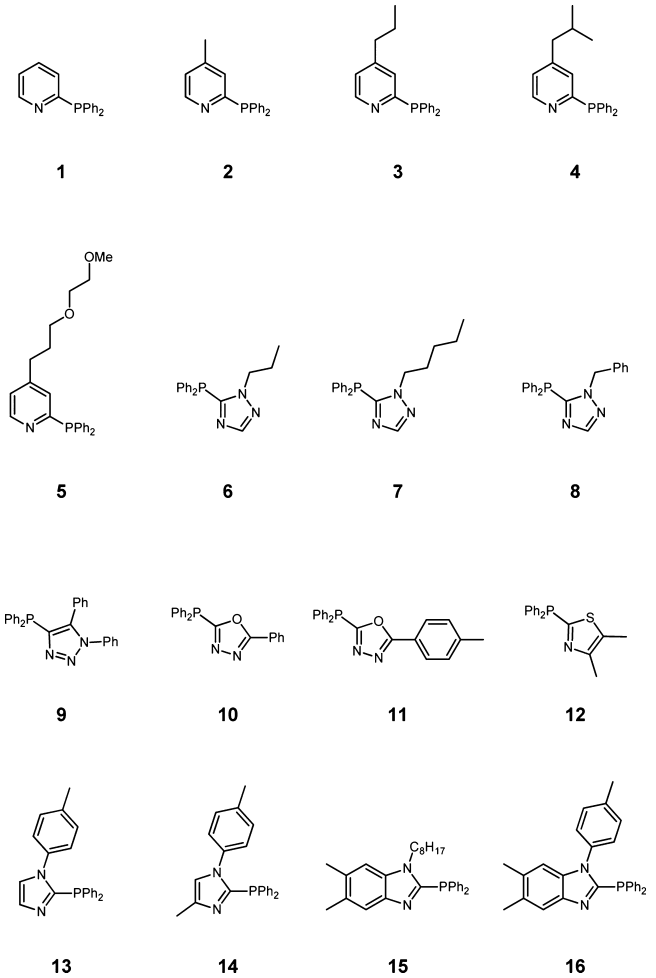

[a]Additional alkyl substituents were introduced for better solubility and processability.

Scheme 1. Synthesis of P^N-Type Ligands 1−16[a]

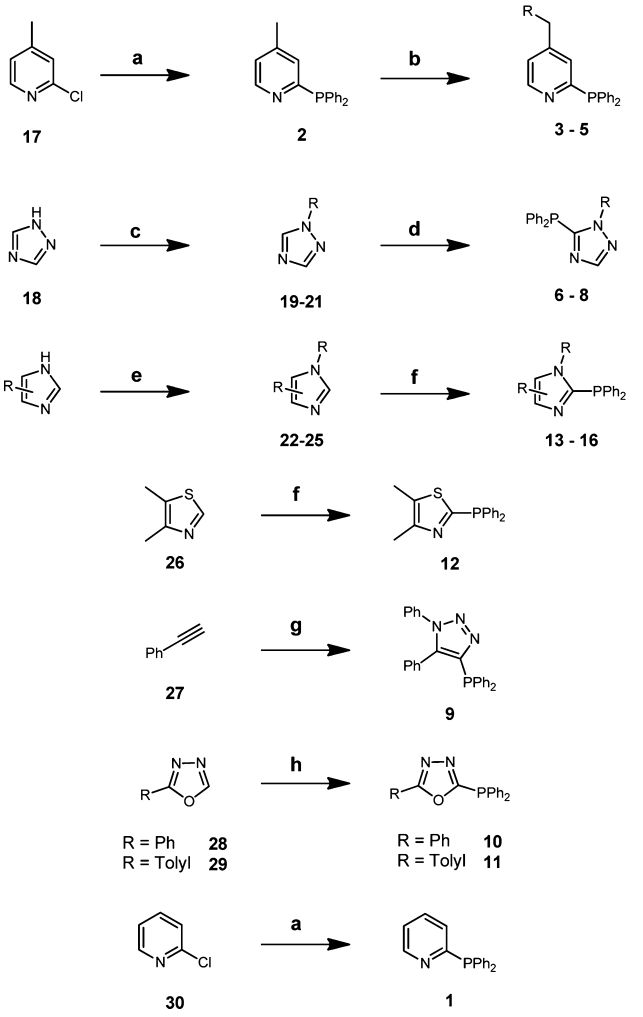

[a]Reagents and conditions: (a) $LiPPh_2$, THF, rt, 8 h; (b) (1) LDA, THF, −78 °C, (2) R-X, −78 °C to rt; (c) DBU, R-X, THF, rt; (d) (1) LDA, THF, −78 °C, (2) Ph_2PCl, −78 °C to rt; (e) NaOH, DMSO, rt; R-X; (f) (1) *n*-BuLi, −78 °C, (2) Ph_2PCl, −78 °C to rt; (g) (1) EtMgBr, THF, rt to 50 °C, (2) PhN_3, rt to 50 °C, (3) Ph_2PCl, rt; (h) NEt_3, Ph_2PCl, pyridine, rt.

The syntheses of the ligands were carried out in one- or two-step reactions according to literature-known processes. Ligands **1** and **2** can be synthesized starting from the appropriate 2-chloropyridine precursor through the reaction with lithium diphenylphosphanide. In the case of ligands **3** and **4**, the extension of the alkyl chain was conducted after the introduction of the phosphine moiety through deprotonation of the methyl group with lithium diisopropylamide and reaction with the appropriate alkyl halide. Ligands with triazole, imidazole, and benzimidazole moieties are accessible by introducing the alkyl substituents in a substitution reaction followed by the introduction of the diphenylphosphino group via deprotonation of the corresponding precursor with *n*-butyllithium and reaction with chlorodiphenylphosphane. 1,2,3-Triazoles can be synthesized in a one-pot procedure out of phenylazide, phenylacetylene, and chlorodiphenylphosphane, whereas oxadiazoles and thiazoles are accessible via one-step reactions starting from literature-known precursor molecules (Scheme 1).[32,62] All P^N ligands were obtained in moderate to good yields and were fully characterized by standard chemical analysis (NMR, MS, and IR). It should be noted that both the synthesis of the chromophoric ligands and their subsequent complexation (vide infra) can be performed on multigram scales at constantly high reaction yields.

Because of its increased stability against oxidation processes, copper(I) iodide was used for complexation reactions instead of copper(I) bromide and copper(I) chloride. However, to investigate additionally the influence of the ligand field strength of the different halides on the photophysical properties, complexes with the full set of the respective copper halides (iodide, bromide, and chloride) have been synthesized for one representative ligand. To synthesize the complexes, the appropriate P^N ligand was mixed together with triphenylphosphine and the metal salt in a 1:2:2 ratio in dichloromethane at room temperature and stirred for several hours (Scheme 2). A completed formation of products was indicated by a clearing of the reaction mixture. Pure compounds were obtained by repeated precipitation of the filtered reaction mixture with diethyl ether or hexane and subsequent washing with the solvent used for precipitation. Crystallization of the complexes for X-ray analysis was achieved by slow diffusion of diethyl ether into the reaction mixture as well as into a

dx.doi.org/10.1021/cm4018375 | *Chem. Mater.* XXXX, XXX, XXX−XXX

Scheme 2. General Procedure for the Synthesis of Heteroleptic, Dinuclear Copper(I) Complexes

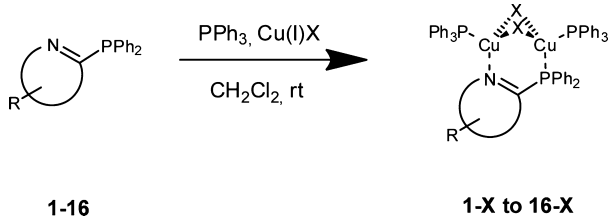

saturated dichloromethane solution. Characterization of the complexes was carried out by mass spectroscopy, elemental analysis, and single-crystal X-ray diffraction (for complexes **2-I**, **11-I**, **12-I**, **13-I**, **14-I**, and **16-I**), which confirmed a general 1:2:2 stoichiometry for all compounds.

3.2. Structural Studies. X-ray structure analyses confirm a binuclear complex structure containing a Cu_2X_2 metal-halide core, one P^N ligand, and two phosphine ligands, as indicated by elemental analysis. The Cu_2X_2 core shows a butterfly shaped structure surrounded by the three ligands. The P^N ligand acts as bridging ligand between the two copper centers, whereas the phosphine ligands coordinate via their phosphorus atom to obtain an approximately tetrahedral coordination for both copper ions. The crystal structure of complex **2-I** is shown in Figure 1.

The general structure of the complexes presented in this study is not affected by the nature of the heterocycle in the bridging ligand. Therefore, a replacement of the six-member heterocycles (e.g., pyridyl species) by five-member heterocycles (e.g., triazoles, benzimidazoles, or thiazoles) is possible without changing the butterfly shape of the copper-halide core (Figure 1, complexes **12-I**, **13-I**, **14-I**, and **16-I**).

The tetrahedral coordination of the copper(I) atom is not surprising because many mononuclear copper(I) complexes as well as polynuclear copper(I) clusters do show this type of geometry.[46] However, the butterfly shaped metal-halide core is in contrast to the typical planar Cu_2X_2 geometry observed for many halogen-bridged Cu_2X_2-type structures.[33,90,93,94]

Selected bond lengths and angles of the investigated complexes are given in Tables 1 and 2. The copper−copper distance of all analyzed complexes is in the range of 2.76−2.89 Å, which is on the order of the sum of the van der Waals radii (2.80 Å).[95] Accordingly, these measured distances are too large for effective metallophilic interactions.[33] Obviously, the copper−copper distances are only negligibly affected by the nature of the bridging heterocycles (i.e., five-member or six-member ring systems). The copper-halide distances differ only slightly within each particular complex, with values in the range of 2.63−2.78 Å. The copper−phosphorus distance Cu(1)−P(1) is slightly longer than Cu(2)−P(2), which can be attributed to the electronegativity of the nitrogen atom.[32] In addition, the copper−nitrogen distance is shorter on average by 0.2 Å compared to the corresponding copper−phosphorus distance.

Each complex shows a slightly distorted tetrahedral geometry around the copper atoms, as is revealed by analyzing the relevant bond angles. All measured bond distances and angles are comparable to the corresponding values found in the homoleptic dinuclear complexes, indicating that the exchange of the two monodentate P^N ligands in the homoleptic complex for two triphenylphosphine ligands influences only slightly the complex structure.[32] The steric influence of a

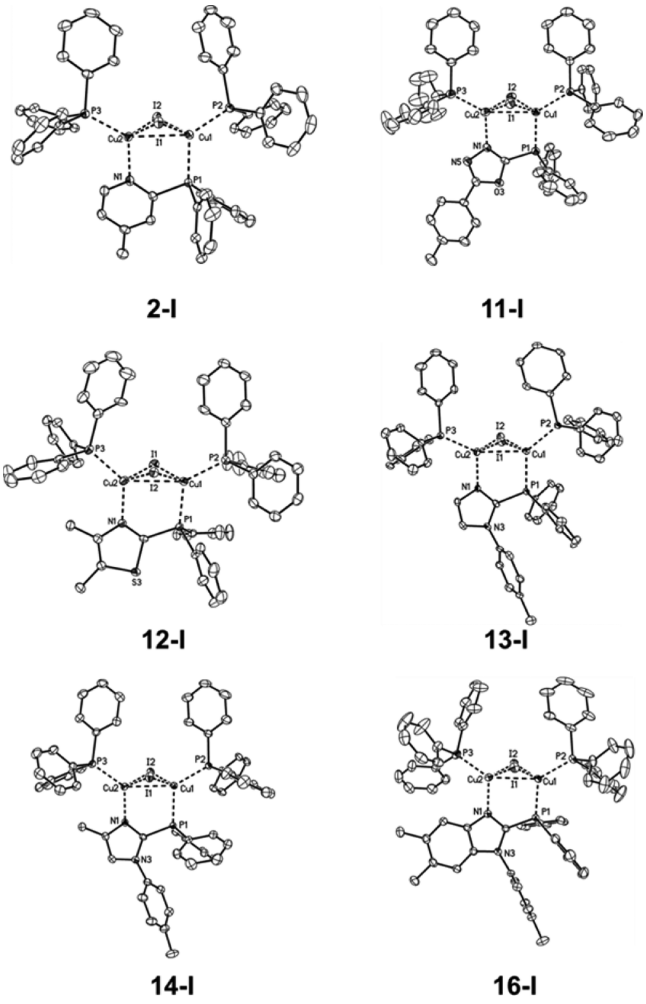

Figure 1. Molecular structure of complexes **2-I**, **11-I**, **12-I**, **13-I**, **14-I**, and **16-I** (hydrogen atoms and minor disordered parts are omitted for clarity, and displacement parameters are drawn at the 50% probability level).

methyl substituent in the ortho position to the nitrogen atom can be seen by comparing the N(1)−Cu(2)−P(3) angle of complexes **13-I** and **14-I**. This angle is widened in complex **14-I** (125.9°) compared to complex **13-I** (115.19°) without a methyl substituent. Bond distances of **13-I** and **14-I**, however, are hardly affected by such a substitution pattern.

3.3. Photophysical Characterization. Absorption measurements for representative examples of each heterocycle (i.e., complexes bearing pyridylphosphine (**2-I**), triazolylphosphine (**8-I** and **9-I**), oxadiazolylphosphine (**10-I**), thiazolylphosphine (**12-I**), and imidazolylphosphine (**13-I** and **16-I**) as the bridging ligand) were recorded in dichloromethane solution at room temperature. The spectra of complex **2-I** together with the free ligand **2** and PPh_3 is shown in Figure 2 and is discussed here as a representative example, whereas the spectra of complexes **8-I**, **9-I**, **10-I**, **12-I**, **13-I**, and **16-I** along with those of their corresponding free ligands can be found in Figures S2−S7 in the Supporting Information. Electronic absorption maxima and extinction coefficients of compounds **2**, **2-I**, **8**, **8-I**, **9**, **9-I**, **10**, **10-I**, **12**, **12-I**, **13**, **13-I**, **16**, **16-I**, and PPh_3 are summarized in Table 3.

Complex **2-I** shows a rather unstructured spectrum, whereas the corresponding spectra of ligand **2** and PPh_3 are more

dx.doi.org/10.1021/cm4018375 | Chem. Mater. XXXX, XXX, XXX−XXX

Table 1. Selected Bond Lengths (Å) of Structurally Characterized $(PPh_3)_2(P\text{^}N)Cu_2I_2$ Complexes

	2-I[a]	11-I	12-I	13-I	14-I	16-I
Cu(1)−Cu(2)	2.816(1) [2.882(6)]	2.877(1)	2.886(1)	2.759(1)	2.818(1)	2.787(1)
Cu(1)−I(1)	2.686(1)	2.671(1)	2.677(1)	2.689(1)	2.647(1)	2.654(1)
Cu(1)−I(2)	2.688(1)	2.674(1)	2.704(1)	2.700(1)	2.678(1)	2.640(1)
Cu(2)−I(1)	2.631(1) [2.534(6)]	2.668(1)	2.694(1)	2.724(1)	2.783(1)	2.681(1)
Cu(2)−I(2)	2.675(1) [2.526(6)]	2.690(1)	2.681(1)	2.628(1)	2.677(1)	2.686(1)
P(2)−Cu(1)	2.249(1)	2.255(1)	2.268(1)	2.271(1)	2.267(1)	2.245(1)
P(1)−Cu(1)	2.235(1)	2.258(1)	2.252(2)	2.278(1)	2.273(1)	2.251(1)
P(3)−Cu(2)	2.253(1) [2.025(6)]	2.215(2)	2.243(1)	2.225(1)	2.240(1)	2.232(1)
N(1)−Cu(2)	2.090(2) [2.861(7)]	2.052(4)	2.073(3)	2.049(3)	2.050(2)	2.052(2)

[a]Data for the minor isomer (6%) is shown in brackets. For the crystal structure, see Supporting Information Figure S1.

Table 2. Selected Bond angles (Degrees) of Structurally Characterized $(PPh_3)_2(P\text{^}N)Cu_2I_2$ Complexes

	2-I[a]	11-I	12-I	13-I	14-I	16-I
I(1)−Cu(1)−I(2)	106.24(1)	106.88(2)	108.50(2)	109.19(2)	111.38(1)	108.92(1)
I(1)−Cu(2)−I(2)	108.21(2) [116.3(2)]	106.47(3)	108.67(2)	110.28(2)	107.30(1)	106.73(1)
Cu(1)−I(1)−Cu(2)	63.95(1) [66.9(1)]	65.22(2)	64.99(2)	61.28(2)	62.45(1)	62.97(1)
Cu(1)−I(2)−Cu(2)	63.36(1) [67.0(1)]	64.87(2)	64.79(2)	62.35(2)	63.49(1)	63.09(1)
P(1)−Cu(1)−I(1)	105.02(2)	105.15(4)	97.77(3)	105.90(3)	99.33(2)	110.77(2)
P(1)−Cu(1)−I(2)	103.09(2)	104.57(4)	103.79(3)	103.16(3)	106.78(2)	99.39(2)
P(2)−Cu(1)−P(1)	123.90(3)	121.22(5)	121.12(4)	128.97(5)	121.12(2)	122.30(2)
P(1)−Cu(1)−Cu(2)	87.16(2) [102.9(1)]	89.62(4)	85.56(3)	89.13(3)	87.31(2)	88.62(2)
N(1)−Cu(2)−P(3)	120.09(6) [99.3(3)]	119.9(1)	129.08(8)	115.2(1)	125.87(5)	123.78(5)
golding of the Cu_2I_2 moiety[b]	54.5 [24.3]	51.6	46.6	53.6	50.9	54.9

[a]Data for the minor isomer (6%) is shown in brackets. [b]The angle between the planes Cu(1), I(1), I(2) and Cu(2), I(1), I(2).

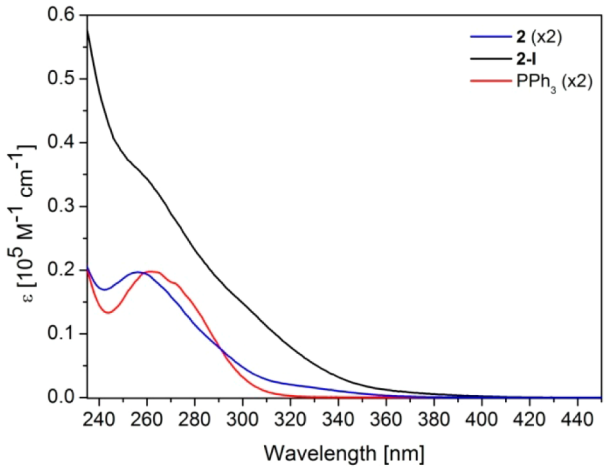

Figure 2. Absorption spectrum of complex **2-I** along with the spectra of the corresponding P^N ligand **2** and PPh_3 at room temperature measured in CH_2Cl_2 solution.

defined. Compound **2-I** exhibits a broad shoulder around 256 nm (ε = 35 878 M^{-1} cm^{-1}), which is assigned to ligand-centered (LC) $\pi-\pi^*$ transitions on the bridging P^N ligand as well as on the monodentate PPh_3. This assumption is supported by the occurrence of corresponding peaks in the free-ligand spectra of **2** and PPh_3 around 256 nm (ε = 9841 M^{-1} cm^{-1}) and 261 nm (ε = 9874 M^{-1} cm^{-1}), respectively. Beyond that, complex **2-I** shows a shoulder around 299 nm (ε = 15 162 M^{-1} cm^{-1}), which is assigned to $\pi-\pi^*$ transitions within the pyridine moiety. Furthermore, additional tails are present in the spectrum of complex **2-I** ranging from approximately 349 to 400 nm (ε = 2034 M^{-1} cm^{-1}), which are not visible in the free-ligand spectra. These low-energy absorption bands are assigned to metal-to-ligand charge-transfer (MLCT) mixed with halogen-to-ligand charge transfer (XLCT) transitions and can therefore be described as (X + M)LCT states,[32] which is in agreement with density functional theory calculations (vide infra). The absorption spectra of complexes **8-I**, **9-I**, **10-I**, **12-I**, **13-I**, and **16-I** exhibit slight differences in the region of 250−300 nm because of different bridging heterocycles and the energetically different π and π^* orbitals. However, the general trends are similar to complex **2-I** and are therefore not discussed in detail.

Emission spectra of neat complex powders were measured at room temperature. For complexes **1-I**, **3-I**, and **4-I** with pyridyl-phosphane ligands, **6-I** and **9-I** with triazolyl phosphine ligands, **10-I** with oxadiazolylphosphine ligands, and **12-I**, **13-I**, **14-I**, and **15-I** with imidazolyl or benzoimidazolyl ligands, the corresponding emission spectra are shown in Figure 3. The spectra of complexes **2-I**, **5-I**, **7-I**, **8-I**, and **16-I** are similar in shape to the spectra shown in Figure 3 and are therefore omitted for clarity, but they can be seen in Figure S8 in the Supporting Information. For a collection of photophysical

dx.doi.org/10.1021/cm4018375 | Chem. Mater. XXXX, XXX, XXX−XXX

Table 3. Extinction Coefficients of Compounds 2, 2-I, 8, 8-I, 9, 9-I, 10, 10-I, 12, 12-I, 13, 13-I, 16, 16-I, and PPh_3[a]

compound	λ_{abs} (nm)	ε (M^{-1} cm^{-1})	assigned transition
2	256	9841	LC, Ph, $\pi-\pi^*$
	291 (sh)	3750	LC, pyridine, $\pi-\pi^*$
2-I	256 (sh)	35 878	LC, Ph, $\pi-\pi^*$
	299 (sh)	15 162	LC, pyridine, $\pi-\pi^*$
	349 (sh)	2034	(X + M)LCT
8	249	11 835	LC, triazole, $\pi-\pi^*$
8-I	250 (sh)	46 814	LC, triazole, $\pi-\pi^*$
	303 (sh)	18 400	(X + M)LCT
9	248 (sh)	23 380	LC, triazole, $\pi-\pi^*$
9-I	305 (sh)	13 384	(X + M)LCT
10	257	22 619	LC, oxadiazole, $\pi-\pi^*$
10-I	262	49 024	LC, oxadiazole, $\pi-\pi^*$
	320	7414	(X + M)LCT
12	273	9647	LC, Ph, $\pi-\pi^*$
	284	9634	LC, thiazole, $\pi-\pi^*$
12-I	260 (sh)	33 280	LC, Ph, $\pi-\pi^*$
	286 (sh)	24 960	LC, thiazole, $\pi-\pi^*$
	334 (sh)	4010	(X + M)LCT
13	255	15 122	LC, Ph, $\pi-\pi^*$
	272 (sh)	10 477	LC, imidazole, $\pi-\pi^*$
13-I	248 (sh)	50 316	LC, Ph, $\pi-\pi^*$
	293 (sh)	18 904	LC, imidazole, $\pi-\pi^*$
	314 (sh)	11 315	(X + M)LCT
16	265 (sh)	15 499	Ph, $\pi-\pi^*$
	300	17 154	LC, benzimidazole, $\pi-\pi^*$
	308 (sh)	15 391	LC, benzimidazole, $\pi-\pi^*$
16-I	296 (sh)	30 729	LC, benzimidazole, $\pi-\pi^*$
	330 (sh)	6500	(X + M)LCT
PPh_3	261	9874	LC, Ph, $\pi-\pi^*$

[a]In dichloromethane solution. sh = shoulder.

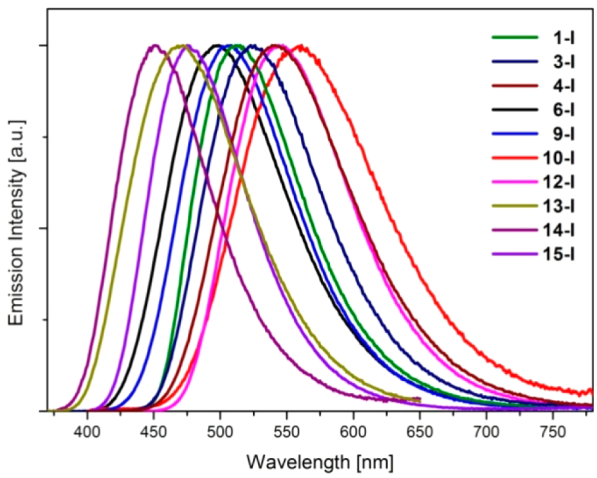

Figure 3. Powder emission spectra of complexes **1-I**, **3-I**, **4-I**, **6-I**, **9-I**, **10-I**, **12-I**, **13-I**, **14-I**, and **15-I** (λ_{exc} = 350 nm, rt).

properties, see Table 4. The emission colors range between 451 nm for compound **14-I** and 558 nm for compound **11-I**.

The spectra of all complexes are broad and unstructured, as observed for their homoleptic counterparts.[32] This is also in accordance with the assumption of (M + X)LCT states as suggested by DFT calculations (i.e., the HOMO being on the metal-halide core and the LUMO on the bridging P^N ligand (vide infra)). Accordingly, the emission characteristics of the

Table 4. Photoluminescence Characteristics[a]

compound	λ_{em} (nm)	Φ_{PL}[b]	τ_{av} (μs)[c]	k_r (10^5 s^{-1})	k_{nr} (10^5 s^{-1})
1-I	514	0.86	2.75	3.13	0.51
1-Br	545	0.70	1.93	3.63	1.55
1-Cl	579	0.42	2.32	1.81	2.50
2-I	515	0.88	3.78	2.33	0.32
3-I	522	0.99	3.05	3.25	0.03
4-I	540	0.91	2.67	3.41	0.34
5-I	552	0.75	2.19	3.42	1.14
6-I	498	0.99	2.96	3.34	0.03
7-I	499	0.72	2.11	3.41	1.33
8-I	506	0.50	2.17	2.30	2.30
9-I	506	0.99	2.85	3.47	0.04
10-I	556	0.85	1.62	5.25	0.93
11-I	558	0.86	3.67	2.34	0.38
12-I	545	0.93	2.52	3.69	0.28
13-I	468	0.72	2.82	2.55	1.00
14-I	451	0.36	1.09	3.30	5.87
15-I	478	0.87	4.22	2.06	0.31
16-I	481	0.91	2.49	3.65	0.36

[a]Neat powders at rt, λ_{exc} = 350 nm. [b]±5% error. [c]Because the decay is best-fitted by bi- or triexponentials, a weighted average lifetime (τ_{av}) is given, which is calculated by the equation $\tau_{av} = \sum A_i\tau_i / \sum A_i$, where A_i is the pre-exponential for lifetime τ_i; the respective values can be seen in Table S2 in the Supporting Information.

complexes can be easily tuned by changing the electronic properties of the bridging P^N ligand.

Complex **1-I** has been chosen as reference compound for the following discussion because it is based on a pyridine heterocycle without any substitution. The emission spectra of compounds with solubilizing alkyl groups (**2-I**–**5-I**) on the pyridine, oxadiazoles (**10-I** and **11-I**), or thiadiazole (**12-I**) ligands are red-shifted relative to **1-I**. On the contrary, compounds with imidazole- (**13-I**–**16-I**) or triazole-based (**6-I**–**8-I**) heterocycles as the bridging ligand show a blue-shift relative to the reference compound. This behavior can be rationalized on the basis of the relative energy content of the heterocycles and the electron-donating or -withdrawing character of the substituents.

The emission wavelength is mainly dependant on the nature of the heterocycle of the bridging P^N ligand. Complexes **1-I**–**5-I** with pyridylphosphane ligands show emission maxima in the range of 514–552 nm, whereas complexes with lower LUMO energies because of their electron-poor character, such as oxadiazoles (**10-I** and **11-I**) or thiadiazole (**12-I**), are red-shifted with emission maxima of 556, 558, and 545 nm, respectively.[96] Accordingly, complexes with high LUMO energies like imidazoles (**13-I** and **14-I**), benzimidazoles (**15-I** and **16-I**), or triazoles (**6-I**, **7-I**, **8-I**, and **9-I**) show blue-shifted emission maxima in the range of 451–506 nm. More precisely, complexes **6-I**, **7-I**, and **8-I**, bearing different alkyl substituents at the nitrogen atom of the triazolyl moiety, show emission maxima at 498, 499, and 506 nm, respectively. By comparing a 1,2,4-triazolyl with a 1,2,3-triazolyl moiety, only small differences can be seen because both kinds of complexes show emission maxima roughly around 500 nm, such as complex **6-I** (1,2,4-triazolyl) and complex **9-I** (1,2,3-triazolyl) with emission maxima at 498 and 506 nm. Complexes bearing an imidazolyl moiety feature emission maxima in the range of 451–481 nm. Again, the influence of the nature of the heterocycle is obvious because for complexes **13-I** or **14-I** with

dx.doi.org/10.1021/cm4018375 | Chem. Mater. XXXX, XXX, XXX–XXX

Table 5. Calculated and Experimental Excitation and Emission Energies (in eV) of Compounds 2-I, 12-I, 13-I, 14-I, and 16-I

compound	$\Delta SCF_{exc,\ BP86}$	$\Delta E_{exc,\ TD\text{-}B3LYP}$	$\Delta E_{abs,\ exp}$	$\Delta SCF_{em,\ BP86}$	$\Delta E_{em,\ TD\text{-}B3LYP}$	SF-TDA	$\Delta E_{em,\ exp}$
2-I	2.29	S_1: 2.31 T_1: 2.29	3.55	1.57	S*1*: 1.51 T_1: 1.46	2.37	2.44
12-I	2.38	S_1: 2.37 T_1: 2.35	3.71	1.52	S_1: 1.42 T_1: 1.36	2.31	2.27
13-I	2.52	S_1: 2.79 T_1: 2.78	3.95	1.64	S_1: 1.65 T_1: 1.60	2.39	2.64
14-I	2.57	S1: 2.90 T_1: 2.88	*a*	1.79	S_1: 1.85 T_1: 1.81	2.47	2.75
16-I	2.43	S_1: 2.54 T_1: 2.53	3.76	1.60	S_1: 1.62 T_1: 1.58	2.37	2.59

[a]Not determined.

electron-rich imidazolyl heterocycles, emission maxima at 468 and 451 nm can be found, respectively, whereas complexes with benzimidazoyl moieties show emission maxima at 478 nm (**15-I**) and 481 nm (**16-I**). This can be explained with the extended aromatic system of the bridging ligand in the case of complexes **15-I** and **16-I**, which results in a lower LUMO energy of the corresponding complexes. The difference in the luminescence maxima of complexes **13-I** (468 nm) and **14-I** (451 nm) can be explained by steric influences because complex **14-I** has a methyl substituent in the ortho-position to the nitrogen atom, leading to a slight distortion in the complex structure (Tables 1 and 2). In detail, the copper−copper distance increase from 2.759 (**13-I**) to 2.818 Å (**14-I**), whereas the P(2)−Cu(1)−P(1) bond angle decreases (128.97° for **13-I** and 121.12° for **14-I**), and the N(1)−Cu(2)−P(3) bond angle increases (115.2° for **13-I** and 125.87° for **14-I**). This observed trend in the emission maxima is also supported by DFT investigations (vide infra) with a calculated distance between the corresponding emission maxima of 17 nm, which is comparable to the value obtained from the experimental measurements (17 nm) (for exact values see Table 5).

DFT investigations of complexes **2-I**, **12-I**, **13-I**, **14-I**, and **16-I** using the B3LYP functional indicate that the observed transitions in fact have mainly (M + X)LCT character. As can be seen in Figure 4, the HOMO is located on the Cu_2I_2 core, whereas the LUMO resides mainly on the bridging P^N ligand. Therefore, modifications of the bridging P^N ligand influence the LUMO energy of the complex to a larger extent than the HOMO energy.[32] The calculated orbital energies show that for all complexes with five-member rings (i.e., **12-I**, **13-I**, **14-I**, and **16-I**) a lower energy of the ligand LUMO (−0.89, −0.72, −0.72, and −0.88 eV, respectively) results in a lower energy of the LUMO of the complex (−1.54, −1.06, −0.99,and −1.24 eV, respectively), whereas the HOMO of the complex remains at approximately the same level (−4.58, −4.41, −4.45, and −4.43 eV, respectively). For details, see Table S4 in the Supporting Information.

To gain better insight into the photophysical behavior of these complexes, TD-DFT and spin-flip TDA calculations of **2-I**, **12-I**, **13-I**, **14-I**, and **16-I** were performed and compared to the experimental values (Table 5). Excitation energies were calculated at the BP86-optimized ground-state structure. The BP86-optimized triplet geometry was used to calculate emission energies following the assumption that the molecule relaxes in the excited state after vertical excitation. Excitation and emission energies were calculated both as energy differences between the closed-shell singlet state and the lowest triplet state (ΔSCF approach) and by using TD-DFT. Because of the charge-transfer character of the excitations, the TD-B3LYP

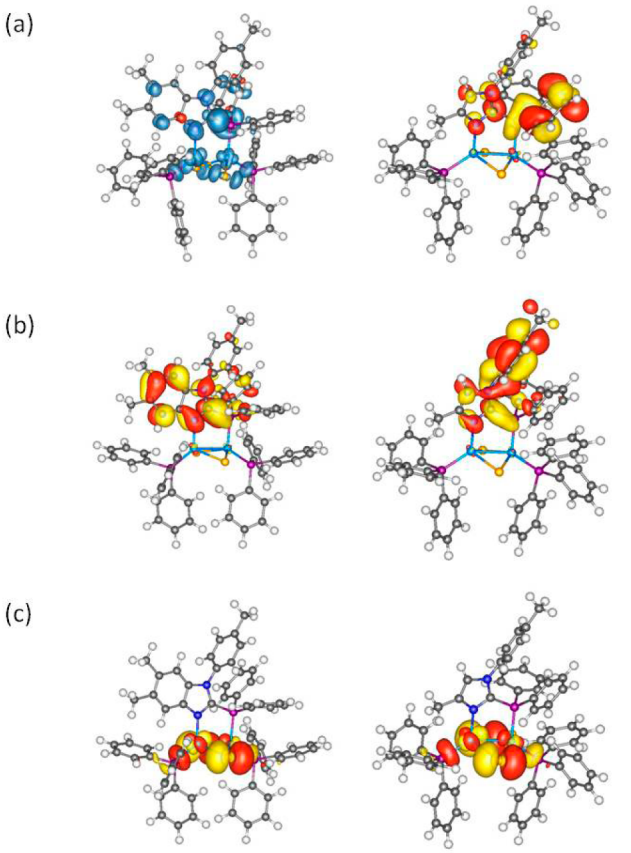

Figure 4. Spin density and frontier orbital plots of complexes **14-I** and **16-I**. Left: (a) Spin density, (b) LUMO, and (c) HOMO of **16-I**. Right: (a) LUMO + 1, (b) LUMO, and (c) HOMO of **14-I**.

excitation energies are much lower than the experimental values. It has been shown previously that the spin-flip Tamm−Dancoff approximation (SF-TDA) yields phosphorescence energies that correlate much better with the experimentally observed emission wavelengths.[78] For the compounds studied in this work, the deviation between the computed and experimental emission wavelength is less than 50 nm, whereas the energies obtained using TD-B3LYP and the ΔSCF approach can be red-shifted even into the infrared region of the spectrum. Despite these limitations, to gain accurate absolute values, the computed absorption and emission wavelengths follow the experimental trend regardless of the particular approach used.

TD-B3LYP calculations in this work and in previous studies indicate that the lowest excited singlet and triplet state of the

dx.doi.org/10.1021/cm4018375 | Chem. Mater. XXXX, XXX, XXX−XXX

Table 6. Character of Lowest TD-B3LYP Singlet and Triplet Excitations

compound	state	E_{exc} (eV)	character	E_{em} (eV)	character
2-I	S_1	2.31	98.7% HOMO → LUMO	1.51	98.6% HOMO → LUMO
	T_1	2.29	98.1% HOMO → LUMO	1.46	97.3% HOMO → LUMO
12-I	S_1	2.37	98.5% HOMO → LUMO	1.42	98.2% HOMO → LUMO
	T_1	2.35	97.7% HOMO → LUMO	1.36	96.8% HOMO → LUMO
13-I	S_1	2.79	82.4% HOMO → LUMO	1.65	98.4% HOMO → LUMO
			9.5% HOMO → LUMO + 2		
	T_1	2.77	79.7% HOMO → LUMO	1.60	97.4% HOMO → LUMO
			11.7% HOMO → LUMO + 2		
14-I	S_1	2.90	71.0% HOMO → LUMO	1.85	98.6% HOMO → LUMO
			23.5% HOMO → LUMO + 1		
	T_1	2.88	67.8% HOMO → LUMO	1.81	97.6% HOMO → LUMO
			25.1% HOMO → LUMO + 1		
16-I	S_1	2.54	98.3% HOMO → LUMO	1.62	98.8% HOMO → LUMO
	T_1	2.53	97.8% HOMO → LUMO	1.58	98.1% HOMO → LUMO

present kind of dinuclear copper complexes can usually be described as a HOMO − LUMO excitation.[32] Only for complexes **13-I** and **14-I** in their respective ground-state structure was a notable influence of other orbitals was found: the excitation from the HOMO to the LUMO is mixed with the excitation from the HOMO to the LUMO + 1 or the LUMO + 2 for **14-I** and **13-I**, respectively (Table 6). Because these higher virtual orbitals are also located on the bridging P^N ligand, this does not change the (M + X)LCT character of the excitation (Figure 4, right).

In addition to these luminescence characteristics concerning different emission maxima, the emission quantum yields and excited-states lifetimes of these complexes were also investigated. Emission quantum yields of neat powders are remarkably high, reaching values between 75 and 99% for pyridylphosphane-based complexes (**1-I**−**5-I**), 50 and 99% for triazole-based complexes (**6-I**−**9-I**), and 36 and 91% for imidazole-based complexes (**13-I**−**16-I**). Oxadiazole-based complexes (**10-I** and **11-I**) show quantum yields of 85 and 86%, respectively, and the thiazole-based complex **12-I** features a quantum yield of 93% (Table 4). These quantum yields are comparable to the values reported for similar dinuclear complexes.[32,36,90]

In detail, pyridylphosphine-based complexes **1-I**, **2-I**, **3-I**, **4-I**, and **5-I** show quantum yields of 86, 88, 99, 91, and 75%, respectively, which are, in general, higher than the values reported for the corresponding homoleptic, dinuclear complexes.[32,97] The emission decay times are in the range of 1.93−3.78 μs, which is somewhat shorter compared to their homoleptic counterparts, resulting in higher radiative rate constants (Table 4). For the homoleptic complexes, an increase of emission quantum yield with increasing size of the alkyl chains used as substituents on the pyridine ring was tentatively found to be due to a more distinct hindrance with respect to geometry changes upon excitation as a result of the more space-demanding alkyl substituents.[32] This trend can also be seen for the heteroleptic complexes **1-I**−**5-I**; however, because these compounds bear two ancillary triphenylphosphine ligands instead of two ancillary P^N ligands, these effects seem not to be influenced by the nature of the ancillary ligands.[61]

Complexes with a 1,2,4-triazolyl moiety (complexes **6-I**, **7-I**, and **8-I**) show quantum yields of 99, 72, and 50%, respectively, together with excited state lifetimes of 2.96, 2.11, and 2.17 μs. The radiative rate constants stay roughly at the same value (3.34×10^5, 3.41×10^5, and 2.30×10^5 s^{-1}, respectively), whereas the nonradiative rate constants increase by 1 or 2 orders of magnitude when going from alkyl (**6-I** and **7-I**) to benzyl (**8-I**) substituents (0.03×10^5, 1.33×10^5, and 2.30×10^5 s^{-1}, respectively). Obviously, structural changes upon excitation leading to a higher nonradiative rate constant and therefore to a lower quantum yield can occur to a larger extent in complex **8-I** as compared to complexes **6-I** and **7-I** because of the different substitution pattern.[32]

Complexes **13-I** and **14-I**, both bearing an imidazolylphosphane as bridging ligand, show significantly different emission quantum yields of 72 and 36% and excited-state lifetimes of 2.82 and 1.09 μs, respectively. Although the radiative rate constants of both complexes are comparable (2.55×10^5 and 3.30×10^5 s^{-1}, respectively), the nonradiative rate constants differ by a factor of 6 (1.00×10^5 and 5.87×10^5 s^{-1}, respectively). Therefore, the additional methyl group ortho to the coordinating nitrogen atom on ligand **14** (cf. ligand **13**) not only influences the emission maxima of the complex but also the emission quantum yields and the excited-state lifetimes.

Benzimidazoylphosphane complexes **15-I** and **16-I** show high quantum yields of 87 and 91% together with decay times of 4.22 and 2.49 μs, respectively. The influence of the two different substituents on the emission maxima is negligible because both are almost identical; however, complex **16-I** with a *p*-tolyl substituent shows a higher radiative rate constant (3.65×10^5 s^{-1}) compared to complex **15-I** with an octyl substituent (2.06×10^5 s^{-1}). Obviously, a more rigid substituent, such as *p*-tolyl, enhances the radiative rate constant and reduces the decay time.

To summarize, the excited-state lifetimes of all complexes measured as neat powders are in the range of 1−4 μs with rate constants for the radiative decay between 2×10^5 and 5×10^5 s^{-1} and for the nonradiative decay between 0.03×10^5 and 5.8×10^5 s^{-1} (Table 4). These values are comparable to those found for the corresponding homoleptic complexes and moreover these decay times are in the range of Pt(II) complexes, which have already been used with good efficiencies in OLEDs.[19,22,32]

To examine the effect of different environments, the photoluminescence properties of complexes **2-I**, **3-I**, **4-I**, **6-I**, **13-I**, and **16-I** were measured in a degassed dichloromethane solution, as a neat film, and as 50% dopant in a PMMA matrix in addition to the powder measurements mentioned above. Figure 5 shows the emission spectra of complex **4-I** in these different environments as a representative example. The

dx.doi.org/10.1021/cm4018375 | Chem. Mater. XXXX, XXX, XXX−XXX

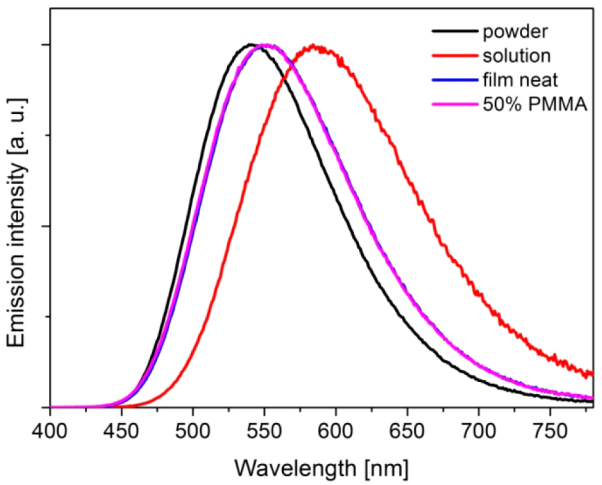

Figure 5. Photoluminescence spectra of complex **4-I** in different environments: powder, CH_2Cl_2 solution, neat film, and PMMA (50%) (λ_{exc} = 350 nm).

corresponding spectra of complexes **2-I**, **3-I**, **6-I**, **13-I**, and **16-I** can be seen in Figures S9−S13 in the Supporting Information. Emission maxima, quantum yields, lifetimes, and rate constants are summarized in Table 7.

The emission maxima of all measured complexes are red-shifted in neat films and PMMA matrix compared to powder measurements. The largest red shifts are observed when the emission is measured in solution. Complexes **2-I**, **3-I**, and **4-I** differ only in the kind of substituent in the 4-position of the pyridine moiety and can therefore be compared directly to each other. As neat powders, these complexes feature emission maxima of 515, 522, and 540 nm, respectively.[96] In neat films as well as doped in PMMA matrix, these emission maxima cover a smaller range of 548−551 nm. The same trends are observed in solution, where the emission maxima are 593, 587, and 586 nm for complexes **2-I**, **3-I**, and **4-I**, respectively. The red-shifts of the emission maxima of the complexes **2-I**, **3-I**, and **4-I** are in the range of 11−35 nm for film or matrix measurements and 46−78 nm for solution measurements compared to the respective emission maxima of neat powders. Thus, the influence of the substituent in the 4-position of the pyridine ring seems to decrease in less rigid environments like neat films, PMMA matrices, and solutions. Compounds **3-I** and **4-I** with longer alkyl chains compared to complex **2-I** show higher quantum yields in powder (99, 91, and 88%, respectively), film (78, 70, and 53%, respectively) and matrix (56, 84, and 75%, respectively) measurements, whereas the emission quantum yields of these complexes are equal in solution (8, 7, and 7%, respectively). The radiative rate constants of complexes **2-I**, **3-I**, and **4-I** are comparable to each other in powder (2.33×10^5, 3.25×10^5, and 3.41×10^5 s^{-1}, respectively) and decrease by 1 order of magnitude in solution (0.59×10^5, 0.63×10^5, and 0.80×10^5 s^{-1}, respectively), whereas the nonradiative rate constant increases by 1 order of magnitude for complex **2-I** (0.32×10^5 to 7.82×10^5 s^{-1}) and 2 orders of magnitude for complex **3-I** and **4-I** (0.03×10 to 7.30×10^5 s^{-1} and 0.34×10^5 to 10.7×10^5 s^{-1}). Obviously, the influences of alkyl chains depend on the environment. In less rigid environments such as solutions, the probability of radiationless deactivation is enhanced in an equal way for all complexes (**2-I**, **3-I**, and **4-I**) independently from the nature of the substituent (i.e., low quantum yields and high nonradiative rate constants), whereas in more rigid environments such as crystal powders, the influence depends on the nature of the alkyl chain: long alkyl chains lead to higher quantum yields and higher radiative rate constants. This is assigned to a more distinct hindrance with respect to geometry changes upon excitation because of the alkyl substituents.[32]

In addition, the emission quantum yields of complex **2-I** are comparable in powder and higher in film, matrix, or solution measurements compared to its corresponding homoleptic counterpart, indicating that the substitution of the two ancillary P^N ligands with triphenylphosphine ligands leads to a more rigid complex structure, which is less vulnerable to structural changes upon excitation and consequently shows an increase of

Table 7. Luminescence Properties of Complexes 2-I, 3-I, 4-I, 6-I, 13-I, and 16-I in Different Environments

	2-I					**3-I**				
complex	λ_{max} (nm)	Φ_{PL} [a]	τ_{av} (μs) [b]	k_r (10^5 s^{-1})	k_{nr} (10^5 s^{-1})	λ_{max} (nm)	Φ_{PL} [a]	τ_{av} (μs) [b]	k_r (10^5 s^{-1})	k_{nr} (10^5 s^{-1})
powder	515	0.88	3.78	2.33	0.32	522	0.99	3.05	3.25	0.03
neat film	550	0.53	2.35	2.26	2.00	548	0.78	2.57	3.04	0.86
50% PMMA	548	0.75	2.28	3.29	1.10	551	0.56	2.37	2.36	1.86
CH_2Cl_2 solution	593	0.07	1.19	0.59	7.82	587	0.08	1.26	0.63	7.30
	4-I					**6-I**				
complex	λ_{max} (nm)	Φ_{PL} [a]	τ_{av} (μs) [b]	k_r (10^5 s^{-1})	k_{nr} (10^5 s^{-1})	λ_{max} (nm)	Φ_{PL} [a]	τ_{av} (μs) [b]	k_r (10^5 s^{-1})	k_{nr} (10^5 s^{-1})
powder	540	0.91	2.67	3.41	0.34	498	0.99	2.96	3.34	0.03
neat film	551	0.70	2.79	2.51	1.08	515	0.72	2.14	3.36	1.31
50% PMMA	551	0.84	2.03	4.14	0.79	513	0.72	2.49	2.89	1.12
CH_2Cl_2 solution	586	0.07	0.87	0.80	10.7	562	0.11	0.99	1.11	8.99
	13-I					**16-I**				
complex	λ_{max} (nm)	Φ_{PL} [a]	τ_{av} (μs) [b]	k_r (10^5 s^{-1})	k_{nr} (10^5 s^{-1})	λ_{max} (nm)	Φ_{PL} [a]	τ_{av} (μs) [b]	k_r (10^5 s^{-1})	k_{nr} (10^5 s^{-1})
powder	468	0.72	2.82	2.55	1.00	481	0.91	2.49	3.65	0.36
neat film	506	0.34	1.65	2.06	4.00	522	0.31	1.35	2.30	5.11
50% PMMA	499	0.44	2.09	2.11	2.68	519	0.69	2.04	3.38	3.24
CH_2Cl_2 solution	544	0.35	1.73	2.02	3.76	554	0.21	1.20	1.75	6.58

[a] ±5% error. [b] Because the decay is best-fitted by bi- or triexponentials, a weighted average lifetime (τ_{av}) is given calculated by the equation $\tau_{av} = \sum A_i\tau_i / \sum A_i$, where A_i is the pre-exponential for the lifetime τ_i; the respective values can be seen in Table S3 in the Supporting Information.

dx.doi.org/10.1021/cm4018375 | Chem. Mater. XXXX, XXX, XXX−XXX

the radiative rate constants and a decrease of the nonradiative rate constants.[32]

The red shift of the emission maxima of neat powder measurements for complexes bearing a triazolylphosphane (**6-I**), an imidazolylphosphane (**13-I**), and a benzimidazoylphosphane (**16-I**) as bridging ligand are in the range of 11−35 nm for neat film measurements and 60−70 nm for solution measurements. These complexes show comparable emission quantum yields in powders (i.e., 99 (**6-I**), 72 (**13-I**), and 91% (**16-I**)) as well as radiative rate constants (i.e., 3.34×10^5 (**6-I**), 2.55×10^5 (**13-I**), and 2.49×10^5 s^{-1} (**16-I**)) to the values obtained for complexes **2-I**, **3-I**, and **4-I**. However, emission quantum yields (11, 35, and 21%) as well as the radiative rate constants (1.11×10^5, 2.02×10^5, and 1.75×10^5 s^{-1}) in solution are an order of magnitude higher compared to the values of pyridylphosphane-based complexes mentioned above. In addition, the nonradiative rate constants are lower, with values of 8.99×10^5 (**6-I**), 3.76×10^5 (**13-I**), and 6.58×10^5 s^{-1} (**16-I**). Therefore, complexes based on five-member heterocycles seem to be less vulnerable to structural changes upon excitation that would lead to an enhanced radiationless deactivation compared to the corresponding complexes based on six-member heterocycles. This characteristic is expressed in higher quantum yields and higher radiative rate constants in solution

In conclusion, both the emission wavelength and the emission quantum yield strongly depend on the environment of the complexes as well as on the substitution pattern and on the nature of the heterocycle of the bridging ligand. By comparing rigid media like crystals with less rigid environments such as neat films, polymer matrices, or solutions, drastic effects can be observed. These changes can be explained with the possibility of larger structural changes upon excitation in these media. In more rigid environments like crystals, the probability of radiationless deactivation is reduced, resulting in significantly higher emission quantum yields.[48] Solutions, in which rearrangements upon excitations can occur more easily, enhance radiationless deactivation processes, leading to a considerable decrease in emission quantum yields.[32] Consequently, in less rigid media, k_{nr} values of the complexes are higher than they are in more rigid environments (Table 7).

The effect of different halides on the photoluminescence properties was studied in the case of the reference structure **1-I** and its analogous structures **1-Br** and **1-Cl**, which all contain 2-diphenylphosphinopyridine as the bridging ligand. The corresponding emission spectra can be seen in Figure 6. A strong red-shift can be observed going from iodide (**1-I**, 514 nm) to bromide (**1-Br**, 545 nm) to chloride (**1-Cl**, 579 nm), which was also observed for comparable dinuclear complexes and was related to the order of the ligand field strength.[32,36] A similar trend is also predicted by DFT calculations for the homologous row of complexes **2-I**, **2-Br**, and **2-Cl**. The calculations were performed on the basis of the crystal structure of complex **2-I** followed by an exchange of the appropriate halides in the copper-halide core because a corresponding crystal structure with ligand **1** was not available for calculations. Calculating the phosphorescence energy of these compounds as the energy difference between the lowest triplet state and the singlet ground state in each case at the optimized triplet geometry (ΔSCF method), the calculated phosphorescence energy decreases from 1.57 eV for **2-I** to 1.48 eV for **2-Cl**. This corresponds well with the experimentally observed red-shift of complexes **1-I**, **1-Br**, and **1-Cl**. The calculated excitation

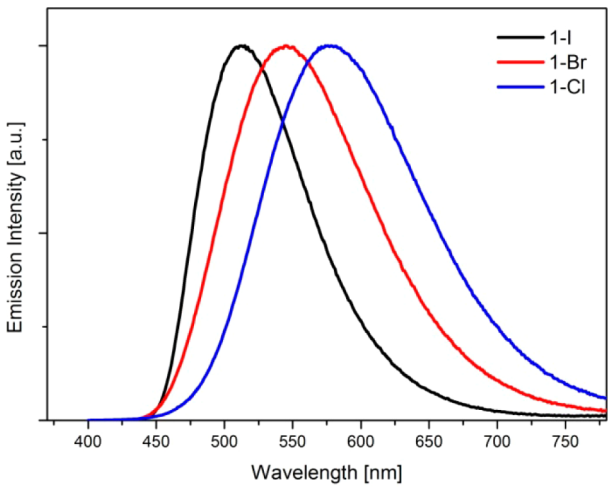

Figure 6. Emission spectra of neat powder of complexes **1-I**, **1-Br**, and **1-Cl** (λ_{exc} = 350 nm).

energies, however, behave inversely and increase from 2.29 eV (**2-I**) to 2.39 eV (**2**-Cl).

3.4. Electroluminescence Studies. Complex **4-I** was used for a test device because of its photophysical properties, excellent quantum yields, and high solubility in the solvent used for device fabrication, namely, toluene. Therefore, approximate HOMO and LUMO energies of complex **4-I** were determined experimentally to choose the appropriate supporting layers. From cyclic voltammetry in dichloromethane with NBu_4PF_6 as the supporting electrolyte and Ferrocene as the internal standard, the energy of the HOMO was determined. For this, we measured the oxidation potential ($E_{p,a}$ = +0.63 V) and calculated the HOMO energy with Andersson's method, CV-$E_{HOMO} = -(E_{p,a}/V + 4.6)$ eV, to be −5.2 eV.[82] This is comparable to the values of related heteroleptic, dinuclear complexes.[61] The LUMO energy was determined using the method of Tauc[83] because of the occurrence of an irreversible reduction process during the cyclic voltammetry measurements, which led to a dissociation of the complex and the deposition of metallic copper on the working electrode. According to the method of Tauc, values for the LUMO energy can be approximated by adding the values for the HOMO and the optical band gaps. Therefore, the energy of the LUMO was calculated to be −2.5 eV.

To estimate the performance of the emitting compound upon electrical excitation, an OLED test device was prepared with the following setup: glass/ITO/PEDOT:PSS (30 nm)/poly-TPD (17 nm)/compound **4-I**:TPBi:PVK 45:45:10 (30 nm)/TPBi (30 nm)/Ca (8 nm)/Ag (100 nm) (Figure 7). The HOMO and LUMO energies of these layers fit well with the corresponding HOMO and LUMO energies of **4-I**. Of these layers, the hole-injection layer (HIL), consisting of PEDOT:PSS, the hole-transport layer (HTL), consisting of poly-TPD, and the emitting layer (EML), consisting of the emitter blend, were deposited from solution by spin-coating. After preparation, the devices were encapsulated by a barrier foil, which was laminated on the top of the bottom-emissive device.

The *I*−*V*−*L* characteristics are presented in Figure 8. The device shows a low turn-on voltage of 4.1 V and a steep increase in luminance, reaching 1800 cd/m^2 at 10 V, which was chosen as the maximum voltage for the measurement. The maximum current efficiency is 9.0 cd/A at 6.3 V and a current

dx.doi.org/10.1021/cm4018375 | *Chem. Mater.* XXXX, XXX, XXX−XXX

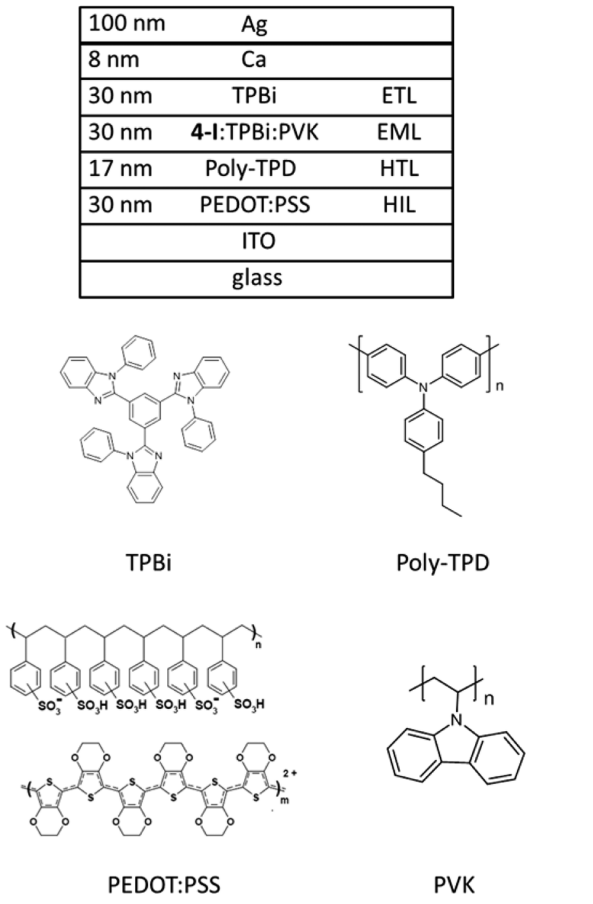

Figure 7. Schematic device structure along with the molecules used for device preparation.

density of 1.6 mA/cm^2. These test-device results demonstrate the outstanding potential of this class of emitting compounds for OLED applications. The high current efficiency of 9.0 cd/m^2 and the turn-on voltage of 4.1 V are a result of the unoptimized device structure, where the triplet energies of host and guest are not well matched. Many copper complexes feature a triplet energy close to 3 eV, whereas the triplet energy of most host- and charge-transport materials is lower. For complex **4-I**, the triplet energy has been estimated to be 2.8 eV from the onset of phosphorescence spectra at 77 K, as proposed by Adachi.[98] This decreases the device efficiency because of an energy transfer from triplet excitons to the host materials.[98−101] The full potential of these materials is still under investigation in other device architectures but is already comparable to solution-processed OLEDs based on copper(I)-emitters, whereas the performance of established Ir(III)- or Pt(II)-systems has not yet been achieved by our system.[35,36,98−102] For Cu(I), solution-based OLEDs have been reported to achieve efficiencies up to 50 cd/A,[98] which is in same range as solution-processed devices with Ir(III)-emitters.[103−106] In work by the group of Adachi,[98] special materials with high triplet energies were used to confine all triplet excitons in the EML. Our goal is to apply this concept to our materials. Currently, our group is working on developing an optimized device architecture to achieve better performance at lower current densities. This extensive work will be published separately.

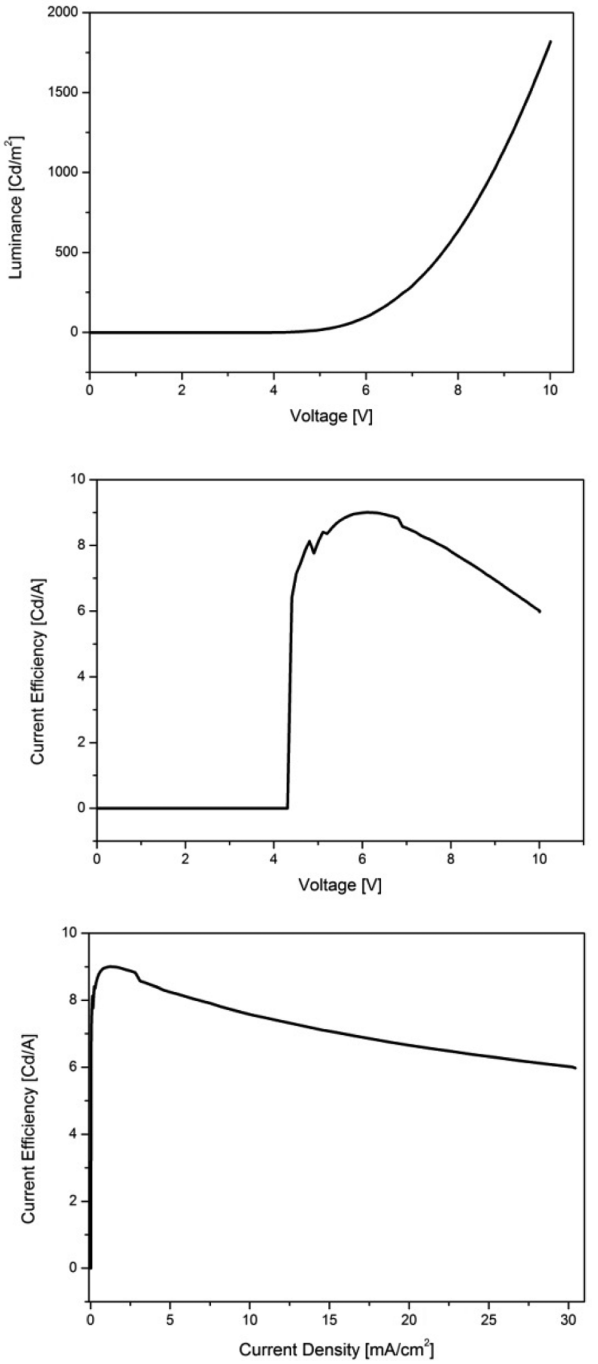

Figure 8. *I*−*V*−*L* characteristics of the test device using complex **4-I** as the emitting compound.

4. CONCLUSIONS

A series of highly luminescent heteroleptic copper(I) complexes was synthesized using a modular approach based on easily accessible P^N ligands, triphenylphosphine, and copper(I) halides. The butterfly shaped structure of the copper(I) halide core is surrounded by one P^N ligand, bridging the two metal centers, and two triphenylphosphine ligands, coordinating via their phosphorus atoms to the copper centers, fulfilling a tetrahedral coordination geometry for each copper atom as revealed by X-ray structure analysis. The photoluminescence characteristics have been investigated,

dx.doi.org/10.1021/cm4018375 | *Chem. Mater.* XXXX, XXX, XXX−XXX

revealing a dependency of the emission maxima and the electronic characteristics of the bridging P^N ligand.

Neat powder measurements show emission maxima ranging from the deep-blue region to the yellow region of the visible spectrum. On one hand, using electron-rich heterocycles (i.e., imidazoles, benzimidazoles, or triazoles), the emission maxima can be shifted to the deep-blue region (451−506 nm). On the other hand, using more electron-poor heterocycles such as pyridine, oxadiazoles, and thiazoles, the emission is red-shifted to the yellow region of the visible spectrum (514−558 nm). These results were also investigated and supported by DFT calculations showing the HOMO being located mainly on the metal-halide core and staying roughly at the same energy level, whereas the energy of the LUMO, which is located on the bridging ligand, depends on this ligand. Therefore, a tuning of the emission maximum by changing the electronic characteristics of the bridging P^N ligand can be achieved.

In addition, the rigidity of the environment also has an influence on the emission of the copper(I) complexes, as shown by investigations of neat powders, neat films, in solution, and doped in PMMA matrices. This is related to a geometry change that occurs upon excitation and thus depends on the rigidity of the environment.

Furthermore, because of their high quantum yields up to 99% and their relatively short emission decay times (1−4 μs), the complexes are promising candidates as OLED emitters. The suitability of a representative complex for OLED application has been successfully demonstrated. Using complex **4-I** as the emitting compound results in a highly green-emitting OLED with a luminance maximum of 1800 cd/m^2 at 10 V. These results confirm the great potential of these complexes, and after carefully optimizing the device architecture, OLEDs based on this class of materials should be able to compete with state-of-the-art emitting materials based on iridium or platinum.

■ ASSOCIATED CONTENT

Supporting Information

Spectroscopic data of compounds **5**−**8** and **11**−**16** as well as additional photophysical spectra together with the Cartesian coordinates (in Å) of the optimized BP86/def2-SV(P) ground-state and triplet geometries of compounds **2-I**, **12-I**, **13-I**, **14-I**, and **16-I** (PDF). This material is available free of charge via the Internet at http://pubs.acs.org. X-ray crystallography data for complexes **2-I**, **11-I**, **12-I**, **13-I**, **14-I**, and **16-I** has been deposited at the Cambridge Crystallography Database under accession numbers CCDC-906844 (**2-I**), CCDC-906845 (**11-I**), CCDC-906849 (**12-I**), CCDC-906847 (**13-I**), CCDC-906848 (**14-I**), and CCDC-906846 (**16-I**).

■ AUTHOR INFORMATION

Corresponding Authors

*E-mail: baumann@cynora.com (T.B.).
*E-mail: braese@kit.edu (S.B.). Fax: (+ 49) 721 608 48581.

Notes

The authors declare no competing financial interest.

■ ACKNOWLEDGMENTS

We acknowledge financial support from KIT. We also thank the Deutsche Forschungsgemeinschaft (DFG) for support, through project B2 of SFB/TRR 88 and the German Federal Ministry of Education and Research (BMBF) in the funding program cyCESH.

■ REFERENCES

(1) You, Y.; Park, S. O. *Dalton Trans.* **2009**, 1267−1282.
(2) Mitschke, U.; Bäuerle, P. *J. Mater. Chem.* **2000**, *10*, 1471−1507.
(3) So, F.; Kido, J.; Burrows, P. *MRS Bull.* **2008**, *33*, 663−669.
(4) *Highly Efficient OLEDs with Phosphorescent Materials*; Yersin, H., Ed.; Wiley-VCH: Weinheim, Germany, 2008.
(5) Loo, Y.-L.; McCulloch, J. *MRS Bull.* **2008**, *33*, 653−662.
(6) Chi, Y.; Chou, P.-T. *Chem. Soc. Rev.* **2010**, *39*, 638−655.
(7) He, L.; Qiao, J.; Duan, L.; Dong, G.; Zhang, D.; Wang, L.; Qiu, Y. *Adv. Funct. Mater.* **2009**, *19*, 2950−2960.
(8) Tsuzuki, T.; Tokito, S. *Adv. Mater.* **2007**, *19*, 276−280.
(9) Yang, C.-H.; Cheng, Y.-M.; Chi, Y.; Hsu, C.-J.; Fang, F.-C.; Wong, K.-T.; Chou, P.-T.; Chang, C.-H.; Tsai, M.-H.; Wu, C.-C. *Angew. Chem., Int. Ed.* **2007**, *46*, 2418−2421.
(10) Lowry, M. S.; Bernhard, S. *Chem.—Eur. J.* **2006**, *12*, 7970−7977.
(11) Ulbricht, C.; Beyer, B.; Friebe, C.; Winter, A.; Schubert, U. S. *Adv. Mater.* **2009**, *21*, 4418−4441.
(12) Lamansky, S.; Djurovich, P. I.; Murphy, D.; Abdel-Razzaq, F.; Kwong, R.; Tsyba, I.; Bortz, M.; Mui, B.; Bau, R.; Thompson, M. E. *Inorg. Chem.* **2001**, *40*, 1704−1711.
(13) Flamigni, L.; Barbieri, A.; Sabatini, C.; Ventura, B.; Barigelletti, F. *Top. Curr. Chem.* **2007**, *281*, 143−203.
(14) Yersin, H.; Rausch, A. F.; Czerwieniec, R. In *Physics of Organic Semiconductors*; Bruetting, W., Adachi, C., Holmes, R. J., Eds.; Wiley-VCH, Weinheim, Germany, 2012; p 371.
(15) Hofbeck, T.; Yersin, H. *Inorg. Chem.* **2010**, *49*, 9290−9299.
(16) Zhou, G.-J.; Wang, X.-Z.; Wong, W.-Y.; Yu, X.-M.; Kwok, H.-S.; Lin, Z. *J. Organomet. Chem.* **2007**, *692*, 3461−3473.
(17) Wong, W.-Y.; He, Z.; So, S.-K.; Tong, K.-L.; Lin, Z. *Organometallics* **2005**, *24*, 4079−4082.
(18) Che, C.-M.; Kwok, C.-C.; Lai, S.-W.; Rausch, A. F.; Finkenzeller, W. J.; Zhu, N.; Yersin, H. *Chem.—Eur. J.* **2010**, *16*, 233−247.
(19) Rausch, A., F.; Murphy, L.; Williams, J. A. G.; Yersin, H. *Inorg. Chem.* **2012**, *51*, 312−319.
(20) Williams, J. A. G. *Top. Curr. Chem.* **2007**, *281*, 205−268.
(21) Williams, J. A. G.; Develay, S.; Rochester, D. L.; Murphy, L. *Coord. Chem. Rev.* **2008**, *252*, 2596−2611.
(22) Kalinowski, J.; Fattori, V.; Cocchi, M.; Williams, J. A. G. *Coord. Chem. Rev.* **2011**, *255*, 2401−2425.
(23) Kim, J. H.; Liu, M. S.; Jen, A. K.-Y.; Carlson, B.; Dalton, L. R.; Shu, C.-F.; Dodda, R. *Appl. Phys. Lett.* **2003**, *83*, 776−778.
(24) Lu, J.; Tao, Y.; Chi, Y.; Tung, Y. *Synth. Met.* **2005**, *155*, 56−62.
(25) Chou, P.-T.; Chi, Y. *Eur. J. Inorg. Chem.* **2006**, 3319−3332.
(26) Breu, J.; Kratzer, C.; Yersin, H. *J. Am. Chem. Soc.* **2000**, *122*, 2548−2555.
(27) Barbieri, A.; Accorsi, G.; Armaroli, N. *Chem. Commun.* **2008**, *19*, 2185−2193.
(28) Hsu, C.-W.; Lin, C.-C.; Chung, M.-W.; Chi, Y.; Lee, G.-H.; Chou, P.-T.; Chang, C.-H.; Chen, P.-Y. *J. Am. Chem. Soc.* **2011**, *133*, 12085−12099.
(29) Czerwieniec, R.; Hofbeck, T.; Crespo, O.; Laguna, A. M.; Concepcion Gimeno, M.; Yersin, H. *Inorg. Chem.* **2010**, *49*, 3764−3767.
(30) Barakat, K. A.; Cundari, T. R.; Omary, M. A. *J. Am. Chem. Soc.* **2003**, *125*, 14228−14229.
(31) Igawa, S.; Hashimoto, M.; Kawata, I.; Hoshino, M.; Osawa, M. *Inorg. Chem.* **2012**, *51*, 5805−5813.
(32) Zink, D. M.; Bächle, M.; Baumann, T.; Nieger, M.; Kühn, M.; Wang, C.; Klopper, W.; Monkowius, U.; Hofbeck, T.; Yersin, H.; Bräse, S. *Inorg. Chem.* **2013**, *52*, 2292−2305.
(33) Zink, D. M.; Baumann, T.; Nieger, M.; Barnes, E. C.; Klopper, W.; Bräse, S. *Organometallics* **2011**, *30*, 3275−3283.
(34) Zhang, L.; Li, B.; Su, Z. *J. Phys. Chem. C.* **2009**, *113*, 13968−13973.
(35) Che, G.; Su, Z.; Li, W.; Chu, B.; Li, M.; Hu, Z.; Zhang, Z. *Appl. Phys. Lett.* **2006**, *89*, 103511-1−103511-3.
(36) Tsuboyama, A.; Kuge, K.; Furugori, M.; Okada, S.; Hoshino, M.; Ueno, K. *Inorg. Chem.* **2007**, *46*, 1992−2001.

(37) Manbeck, G. F.; Brennessel, W. W.; Eisenberg, R. *Inorg. Chem.* **2011**, *50*, 3431−3441.
(38) McMillin, D. R.; Buckner, M. T.; Ahn, B. T. *Inorg. Chem.* **1977**, *16*, 943−945.
(39) Buckner, M. T.; McMillin, D. R. *J. Chem. Soc., Chem. Commun.* **1978**, 759−761.
(40) Blaskie, M. W.; McMillin, D. R. *Inorg. Chem.* **1980**, *19*, 3519−3522.
(41) McMillin, D. R.; Kirchhoff, J. R.; Goodwin, K. V. *Coord. Chem. Rev.* **1985**, *64*, 83−92.
(42) McMillin, D. R.; McNett, K. M. *Chem. Rev.* **1998**, *98*, 1201−1219.
(43) Crane, D. R.; DiBenedetto, J.; Palmer, C. E. A.; McMillin, D. R.; Ford, P. C. *Inorg. Chem.* **1988**, *27*, 3698−3700.
(44) Simon, J. A.; Palke, W. E.; Ford, P. C. *Inorg. Chem.* **1996**, *35*, 6413−6421.
(45) Crestani, M. G.; Manbeck, G. F.; Brennessel, W. W.; McCormick, T. M.; Eisenberg, R. *Inorg. Chem.* **2011**, *50*, 7172−7188.
(46) Ford, P. C.; Cariati, E.; Bourassa. *J.Chem. Rev.* **1999**, *99*, 3625−3647 and references therein.
(47) Hashimoto, M.; Igawa, S.; Yashima, M.; Kawata, I.; Hoshino, M.; Osawa, M. *J. Am. Chem. Soc.* **2011**, *133*, 10348−10351.
(48) Czerwieniec, R.; Yu, J.; Yersin, H. *Inorg. Chem.* **2011**, *50*, 8293−8301.
(49) Czerwieniec, R.; Yu, J.; Yersin, H. *Inorg. Chem.* **2012**, *51*, 1975.
(50) Yersin, H.; Czerwieniec, R.; Hupfer, A. *Proc. SPIE* **2012**, *8435*, 843508-1−843508-10.
(51) Yersin, H.; Rausch, A. F.; Czerwieniec, R.; Hofbeck, T.; Fischer, T. *Coord. Chem. Rev.* **2011**, *255*, 2622−2652.
(52) Bergmann, L.; Friedrichs, J.; Mydlack, M.; Baumann, T.; Nieger, M.; Bräse, S. *Chem. Commun.* **2013**, *49*, 6501−6503.
(53) Gushurst, A. K. I.; McMillin, D. R.; Dietrich-Buchecker, C. O.; Sauvage, J. P. *Inorg. Chem.* **1989**, *28*, 4070−4072.
(54) Miller, M. T.; Gantzel, P. K.; Karpishin, T. B. *J. Am. Chem. Soc.* **1999**, *121*, 4292−4293.
(55) Cuttel, D. G.; Kuang, S.-M.; Fanwick, P. E.; McMillin, D. R.; Walton, R. A. *J. Am. Chem. Soc.* **2002**, *124*, 6−7.
(56) Zhang, Q.; Ding, J.; Cheng, Y.; Wang, L.; Xie, Z.; Jing, X.; Wang, F. *Adv. Funct. Mater.* **2007**, *17*, 2983−2990.
(57) Felder, D.; Nierengarten, J.-F.; Barigelletti, F.; Ventura, B.; Armaroli, N. *J. Am. Chem. Soc.* **2001**, *123*, 6291−6299.
(58) Deaton, J. C.; Switalski, S. C.; Kondakov, D. Y.; Young, R. H.; Pawlik, T. D.; Giesen, D. J.; Harkins, S. B.; Miller, A. J. M.; Mickenberg, S. F.; Peters, J. C. *J. Am. Chem. Soc.* **2010**, *132*, 9499−9508.
(59) Harkins, S. B.; Peters, J. C. *J. Am. Chem. Soc.* **2005**, *127*, 2030−2031.
(60) Corresponding OLED data will be presented elsewhere.
(61) Volz, D.; Zink, D. M.; Bocksrocker, T.; Friedrichs, J.; Nieger, M.; Baumann, T.; Lemmer, U.; Bräse, S. *Chem. Mater.* **2013**, *25*, 3414−3426.
(62) Kawano, T.; Hirano, K.; Satoh, T.; Miura, M. *J. Am. Chem. Soc.* **2010**, *132*, 6900−6901.
(63) Newkome, G. R.; Hager, D. C. *J. Org. Chem.* **1978**, *43*, 947−949.
(64) Liu, D.; Gao, W.; Dai, Q.; Zhang, X. *Org. Lett.* **2005**, *7*, 4907−4910.
(65) Tolmachev, A. A.; Zarudnitskii, E. V.; Yurchenko, A. A.; Pinchuk, A. M. *Chem. Heterocycl. Compd.* **1999**, *35*, 1117−1119.
(66) Bulger, P. G.; Cottrell, I. F.; Cowden, C. J.; Davies, A. J.; Dolling, U.-H. *Tetrahedron Lett.* **2000**, *41*, 1297−1301.
(67) Harkal, S.; Rataboul, F.; Zapf, A.; Fuhrmann, C.; Riermeier, T.; Monsees, A.; Beller, M. *Adv. Synth. Catal.* **2004**, *346*, 1742−1748.
(68) Cheung, H. Y.; Yu, W.-Y.; Lam, F. L.; Au-Yeung, T. T.-L.; Zhou, Z.; Chan, T. H.; Chan, A. S. C. *Org. Lett.* **2007**, *9*, 4295−4298.
(69) Sheldrick, G. M. *Acta Crystallogr.* **2008**, *A64*, 112−122.
(70) Speck, A. L. *Appl. Crystallogr.* **2003**, *36*, 7−13.
(71) Becke, A. D. *Phys. Rev. A* **1988**, *38*, 3098−3100.
(72) Perdew, J. P. *Phys. Rev. B* **1986**, *33*, 8822−8827.
(73) Häser, M.; Ahlrichs, R. *J. Comput. Chem.* **1989**, *10*, 104−111.
(74) Weigend, F.; Häser, M. *Theor. Chem. Acc.* **1997**, *97*, 331−340.
(75) Sierka, M.; Hogekamp, A.; Ahlrichs, R. *J. Chem. Phys.* **2003**, *118*, 9136−9148.
(76) Lee, C.; Yang, W.; Parr, R. G. *Phys. Rev. B* **1988**, *37*, 785−789.
(77) Stephens, P. J.; Devlin, F. J.; Chabalowski, C. F.; Frisch, M. J. *J. Phys. Chem.* **1994**, *98*, 11623−11627.
(78) Kühn, M.; Weigend, F. *Chem. Phys. Chem.* **2011**, *12*, 3331−3336.
(79) Weigend, F.; Ahlrichs, R. *Phys. Chem. Chem. Phys.* **2005**, *7*, 3297−3305.
(80) Rappoport, D.; Furche, F. *J. Chem. Phys.* **2010**, *133*, 134105/1−134105/11.
(81) *TURBOMOLE*, version 6.4; TURBOMOLE GmbH: Karlsruhe, Germany, 2012; http://www.turbomole.com.
(82) Admassie, S.; Inganäs, O.; Mammo, W.; Perzon, E.; Andersson, M. R. *Synth. Met.* **2006**, *156*, 614−623.
(83) Tauc, J.; Grigorovici, R.; Vancu, A. *Phys. Status Solidi B* **1966**, *15*, 627−637.
(84) Kyle, K. R.; Ryu, C. K.; DiBenedetto, J. A.; Ford, P. C. *J. Am. Chem. Soc.* **1991**, *113*, 2954−2965.
(85) Fitchett, C. M.; Steel, P. J. *Inorg. Chem. Commun.* **2007**, *10*, 1297−1300.
(86) Schramm, V.; Pierre, A.; Hiller, W. *Acta Crystallogr.* **1984**, *C40*, 1840−1841.
(87) Hiller, W. *Acta Crystallogr.* **1986**, *C42*, 149−150.
(88) Engelhardt, L. M.; Healy, P. C.; Kildea, J. D.; White, A. H. *Aust. J. Chem.* **1989**, *42*, 913−922.
(89) Maeyer, J. T.; Johnson, T. J.; Smith, A. K.; Borne, B. D.; Pike, R. D.; Pennington, W. T.; Krawiec, M.; Rheingold, A. L. *Polyhedron* **2003**, *22*, 419−431.
(90) Araki, H.; Tsuge, K.; Sasaki, Y.; Ishizaka, S.; Kitamura, N. *Inorg. Chem.* **2005**, *44*, 9667−9675.
(91) Hirtenlehner, C.; Monkowius, U. *Inorg. Chem. Commun.* **2012**, *15*, 109−112.
(92) Eisler, D. J.; Kirby, C. W.; Puddephatt, R. J. *Inorg. Chem.* **2003**, *42*, 7626−7634 and references therein.
(93) Aslanidis, P.; Cox, P. J.; Divanidis, S.; Tsipis, A. C. *Inorg. Chem.* **2002**, *41*, 6875−6886.
(94) Henary, M.; Wootton, J. L.; Khan, A. I.; Zink, J. I. *Inorg. Chem.* **1997**, *36*, 796−801.
(95) Bondi, A. *J. Phys. Chem.* **1964**, *68*, 441−451.
(96) Neat powder measurements of pyridylphosphine-based complexes **1-I**, **2-I**, **3-I**, **4-I**, and **5-I** show emission maxima of 514, 515, 522, 540, and 552 nm, respectively. These complexes carry weak donor substituents such as linear or branched alkyl groups as well as alkoxy groups in the 4 position of the pyridine moiety. As is visible from the data, introduction of weak donor substituents (e.g., alkyl groups) apparently leads to a slightly red-shifted emission maxima, which is in contrast to the expected luminescence behavior. (Introduction of donor substituents should result in a blue-shift of the emission maxima because the higher LUMO energy of the complex leads to a larger HOMO−LUMO gap and thus larger excitation and emission energies.) However, this correlation is obviously oversimplified. Additional effects, especially steric effects like the relaxation in the excited state, seem to overcompensate the predicted blue-shift, which was partially shown at the corresponding homoleptic, dinuclear complexes.[32]
(97) Volz, D.; Nieger, M.; Friedrichs, J.; Baumann, T.; Bräse, S. *Langmuir* **2012**, *29*, 3034−3044.
(98) Zhang, Q.; Komino, T.; Huang, S.; Matsunami, S.; Goushi, K.; Adachi, C. *Adv. Funct. Mat.* **2012**, *22*, 2327−2336.
(99) Zhang, D. *J. Lumin.* **2010**, *130*, 1419−1424.
(100) Sun, W.; Zhang, Q.; Qin, L.; Cheng, Y.; Xie, Z.; Lu, C.; Wang, L. *Eur. J. Inorg. Chem.* **2010**, 4009−4017.
(101) Zhang, L.; Li, B. *J. Electrochem. Soc.* **2009**, *156*, 174−178.
(102) Zhang, Q.; Zhou, Q.; Cheng, Y.; Wang, L.; Ma, D.; Jing, X.; Wang, F. *Adv. Mater.* **2004**, *16*, 432−436.

(103) Lam, E. S.-H.; Tsang, D. P.-K.; Lam, W. H.; Tam, A. Y.-Y.; Chan, M.-Y.; Wong, W.-T.; Yam, V. W.-W. *Chem. Eur. J.* **2013**, *19*, 6385−6397.
(104) Ho, C.-L.; Wong, W.-Y.; Yao, B.; Xie, Z.; Wang, L.; Lin, Z. *J. Organomet. Chem.* **2009**, *694*, 2735−2749.
(105) Zhang, F.; Duan, L.; Qiao, J.; Dong, G.; Wang, L.; Qiu, Y. *Org. Electron.* **2012**, *13*, 1277−1288.
(106) Song, M.; Park, J.; Kim, Y. I.; Lee, J. W.; Jin, S. *Mol. Cryst. Liq. Cryst.* **2012**, *567*, 37−41.